Faculty of Mechanical Engineering

CIRCULAR COMPOSITE TUBES UNDER QUASI-STATIC AXIAL LOADING

Arjun A/L A. Ravindran

Bachelor in Mechanical Engineering

2018

**CIRCULAR COMPOSITE
TUBES UNDER QUASI-STATIC AXIAL LOADING**

ARJUN A/L A. RAVINDRAN

**A thesis submitted
in fulfilment of the requirements for the Bachelor of Mechanical Engineering**

Faculty of Mechanical Engineering

UNIVERSITI TEKNIKAL MALAYSIA MELAKA

2018

DECLARATION

I declare that this thesis entitled "Circular Composite Tubes Under Quasi-Static Axial Loading" is the result of my own research except as cited in the references.

Signature : ....

Name : ....

Date : ....

APPROVAL

I hereby declare that I have read this thesis and in my opinion this thesis is sufficient in terms of scope and quality for the award of the Bachelor of Mechanical Engineering (with Honours).

Signature : ……………………………………………….

Supervisor's Name : ……………………………………………….

Date : ……………………………………………….

ABSTRACT

Composite structures are extensively used in the aerospace and automotive industry, where high amounts of force are involved. Manufacturers are currently venturing into green and ecologically friendly materials such as plant-based fibres and synthetic-plant fibre hybrids to improve crashworthiness of composites. However, these composites still exhibit poor energy absorption characteristics compared to conventional load bearing materials such as metal and have to be improved by altering parameters during the fabrication process. This experiment aims to determine the effects of parameters, specifically triggering mechanism and fibre lay-up sequence on the energy absorption capability of fibre reinforced composites. In this study cross-ply of unidirectional glass (G), banana (B), and glass-banana hybrid fibre reinforced composite tubes were investigated. The composites were fabricated with different fibre lay-up sequence, and each fibre sequence features three different triggering mechanism. Composite specimens were fabricated using the bladder assisted moulding method which utilised a circular tube with 1000 mm in length and 57.30 mm outer diameter. Specimens are 100 mm in length and have an outer diameter of 57.30 mm. Triggering mechanisms tested are flat-end, 45° chamfer and the 4-petal tulip. The specimens are fabricated with GGG lay-up, BBB lay-up, and two hybrid GBG and BGB lay-up configurations. A quasi-static axial crushing test was performed at 10 mm/min with a 150 kN capacity universal testing machine Instron 5585. From the test, it was found that triggered specimens experienced better crushing performance, with the tulip trigger achieving higher values of mean load, specific energy absorption and crush force efficiency compared to the flat-ended and 45° chamfered specimens. In terms of fibre lay-up sequence, hybridisation between banana and glass fibres (GBG and BGB sequence) exhibited better values of parameters tested and displayed stable and progressive crushing during the test.

ABSTRAK

Projek ini melibatkan keupayaan komposit untuk menyerap daya. Struktur-struktur komposit banyak digunakan dalam industri automotif dan aero-angkasa, di mana struktur-struktur tersebut akan didedahkan kepada nilai daya yang tinggi. Pada zaman ini, teknologi bahan mesra alam sedang diberi fokus, terutamanya dalam kajian serat tumbuhan, serat sintetik dan serat hibrid sintetik-tumbuhan. Namun demikian, komposit-komposit tersebut tidak mengemukakan keupayaan menyerap daya sebaik dengan bahan-bahan menyerap daya konvensional seperti besi dan logam, dan parameter-parameter perlu diubah dalam proses fabrikasi komposit. Tujuan kajian ini adalah untuk meneliti kesan-kesan mengubah mekanisma pencetusan daya dan susunan kain serat ke atas keupayaan komposit untuk menyerap daya. Kajian ini melibatkan tiub komposit hibrid yang dibuat daripada tenunan serat semula-jadi pisang (G), serat sintetik kaca dan hibrid antara serat pisang-kaca. Proses fabrikasi komposit menggunakan proses 'bladder assisted moulding' dengan acuan yang mempunyai panjan 1000 mm dan diameter luaran 57.30 mm. Spesimen yang dihasilkan mempunyai panjang 100 mm dan diameter luaran 57.30 mm. Mekanisma pencetusan daya yang dikaji adalah spesimen rata, pemotongan serong 45°, dan tulip dengan 4 kelopak. Susunan kain serat yang dikaji adalah susunan GGG, BBB, dan susunan hibrid GBG dan BGB. Satu ujian hentaman kuasi statik dengan kelajuan 10 mm/min dan sel beban 150 kN telah dijalankan ke atas spesimen mneggunakan mesin penguji sejagat Instron 5585. Data yang diperolehi menunjukkan bahawa mekanisma pencetudan daya tulip mencapai nilai daya purata, penyerapan daya spesifik dan kecekapan tenaga yang tinggi berbanding dengan mekanisma pencetusan daya yang lain. Dari segi susunan kain serat, data menunjukkan bahawa komposit susunan hibrid (susunan GBG dan BGB) mencapai nilai-nilai yang tinggi dalam parameter yang diuji dan menampilkan ciri-ciri hentaman yang stabil dan progresif.

ACKNOWLEDGEMENTS

First and foremost, I would like to thank my final year project supervisor, Assoc. Prof. Dr. Sivakumar A/L Dhar Malingam from the Faculty of Mechanical Engineering, Universiti Teknikal Malaysia Melaka for continuously guiding me throughout the process of completing this research. His time, guidance, advice and support are very much appreciated.

Special appreciation to Universiti Teknikal Malaysia Melaka for giving us, students, the chance to go through the process of completing the Final Year Project. We have gained valuable knowledge and exposure throughout the process of this project. Moreover, this project also gave us the opportunity to use what we have learned in our degree courses in completing this research.

Sincere thanks to PhD student Mr. Ng Ling Feng for sharing his experience and knowledge along this research. I would like to acknowledge his comments and suggestions, which was crucial for the successful completion of this project.

Last but not least, thanks and appreciation to my parents for their constant love and support, both morally and financially. Their hard work and sacrifice have put me where I am today and has enabled me to pursue Mechanical Engineering. No words can come close to expressing my gratitude towards them.

TABLE OF CONTENTS

LIST OF TABLES

LIST OF FIGURES

LIST OF APPENDICES

LIST OF SYMBOLS/ABBREVIATIONS

SEA	-	Specific Energy Absorption
CFE	-	Crush Force Efficiency
FRC	-	Fibre Reinforced Composite
G	-	Glass Fibre
B	-	Banana Fibre
RTM	-	Resin Transfer Moulding
P_{max}	-	Maximum Load
P_{mean}	-	Mean Load
SMA	-	Shape Memory Alloy
Ө	-	Orientation Angle
D/t	-	Diameter to Thickness ratio
CNTs/PSF	-	Carbon Nanotubes/Polysulfone
NT	-	Non-triggered specimens
CT	-	Chamfer-triggered specimens
TT	-	Tulip-triggered specimens

CHAPTER 1

INTRODUCTION

1.1 Background

Crashworthiness is an aspect of kinetic energy absorption that is widely studied and researched, especially in the aerospace and automotive industry. Crashworthiness is the ability of the structure to absorb kinetic energy in a crash situation to protect the components or inhabitants in the structure. It involves the distribution of forces in the event of a crash as long and as widespread as possible to avoid the impact force on a person. Moreover, some studies emphasize the importance of the occupant or component compartments to retain its structural integrity during a crash (Jackson, Dutton, Gunnion, & Kelly, 2011; Ramakrishna & Hull, 1993; Sigalas, Kumosa, & Hull, 1991).

The crashworthiness of a structure can be determined analytically by calculating its specific energy absorption (SEA). It is the energy absorbed per unit mass of crushed material. A structure is said to have good SEA if it fulfils certain criteria, like low total weight, high specific stiffness, and high specific strength (Luo, Yan, Meng, & Jin, 2016). For decades, the automotive and aerospace industry has primarily used metal in building structures and compartments to absorb impact energy. However, recent studies have shown that composite materials with polymers and fibres display improved mechanical properties compared to metal, with a fraction of its weight and cost. In terms of crashworthiness, fibre-polymer composites prove to have more efficient energy dissipation around its structure. This is shown by the SEA values determined by quasi-static axial loading tests (Hosseini & Shariati, 2018).

In the pursuit of green and sustainable technology, researches have focused on the application of natural fibres, and also the hybridisation of natural and synthetic fibres. Natural fibres such as banana fibre are by-products from banana fruit plantations, where the stalk necessary for fibre production can be obtained for free after the fruit is harvested. This process not only reduces the manufacturing cost, but also reduces waste generated from banana plantations (Padam et al., 2014).

Apart from the type of material used, trigger mechanisms applied on the structure have also shown to effect the energy absorption of the structure involved (Siromani et al., 2014). Trigger mechanisms have two types, internal and external triggers. These triggers mainly effect the way the loading is distributed within the structure, with trigger spots absorbing varied amounts of energy (Sivagurunathan et al., 2018) Examples of triggers include chamfered trigger, tulip trigger, plug trigger and crush cap trigger. Studies on trigger mechanisms in composite structures show that it significantly improves the SEA of the structures while reducing overall weight (Eshkoor et al., 2013).

1.2 Problem Statement

As the automotive and aerospace industry expands, the attention on building material is shifting from metals to composite polymers. This is because metals not only cost more, but they also add to the overall weight of the structure. Metals also present the problem of unsuitable mechanical properties. Moreover, the use of metals causes the build-up of rust, which will affect the performance of the structure or mechanism involved. Alternative materials that behave better under loading are being focused on. One such alternative is using composite structures reinforced with fibres.

Extensive research has been conducted on plant fibres mainly due to the inexhaustible supply of plant-based materials. Plant fibres such as kenaf, hemp, and jute are used in numerous studies to test its mechanical properties as a suitable replacement for metal (Alia, Cantwell, Langdon, Yuen, & Nurick, 2014). Synthetic fibres are also in demand, as glass fibre is highly sought after for concrete and composite reinforcement. Specifically, fibres are used to produce fibre reinforced composites (FRC) as metal substitutes for structures and mechanisms. However, these composites exhibit poor energy absorption levels and undergo catastrophic failure when placed under quasi-static axial loading (Jackson et al., 2011). Many factors can affect the failure modes and specific energy absorption (SEA) values obtained by the composites, such as fibre to weight ratio, type of fibre used, fibre orientation, moulding pressure and trigger mechanisms. Studies are required to improve the FRC energy absorption capability.

1.3 Objectives

The objectives of the current research are:

a) To study the crushing behaviour of the fibre reinforced composites with different triggering mechanisms by applying a quasi-static axial crushing test.

b) To study the effects of varying fibre-lay-up on the crushing behaviour of the fibre reinforced composites.

1.4 Scope of Project

The research is divided to two parts. The first part comprises of the fabrication process of the fibre reinforced composites, and the second part focuses on the quasi-static axial crush testing of the FRC components.

For the fabrication of the composites, bladder assisted moulding method is used. Glass fibre (G) and banana fibre (B) will be used to fabricate the composite tubes. Initially, specimens will be fabricated with different fibre lay-up sequences. Internal trigger mechanisms such as chamfered triggers and tulip triggers will then be fabricated. The second phase of the research is the testing phase, where the composite tubes produced will undergo a quasi-static axial loading crush test.

CHAPTER 2

LITERATURE REVIEW

2.1 Introduction

This chapter will focus on the concept of crashworthiness and energy absorption, as well as the factors that influence these values in related literature works. Some of those factors are triggering mechanisms, fibre stacking and geometrical parameters. Before the application of composite materials, metal tubes were heavily and extensively researched to determine their crashworthiness and energy absorbing capabilities in high impact situations. However, metals proved to be heavy and expensive to acquire, as well as laborious in terms of fabrication and machining. Years of research prove that fibre reinforced composite structures were cheaper, easier to fabricate and much more efficient in terms of its crashworthiness and energy absorbing abilities.

2.2 Energy Absorption Classification

Energy absorption represents the rate of which energy can be dissipated in a specimen in the event of a crush. A high value of energy absorption indicates that a specimen is very efficient in uniformly propagating energy when exposed to loading. However, this parameter does not indicate the specimen's efficiency in terms of vibration dampening, buckling resistance, and other mechanical properties (Stamenovic et.al., 2011).

In a quasi-static crushing test, peak load (P_{max}) is denoted as the first maximum value or initial peak of load value in the load vs deformation graph. This value represents the highest value of load the specimen achieves before entering plastic deformation or post-crushing zone.

Mean load (P_{mean}) is the average load sustained by the specimen while the crushing process is in the post-crushing zone. It is determined by the total accumulated load in the post-crushing zone divided by the distance of crushing in the same region, expressed in Eq (2.1):

$$P_{mean} = \frac{\int_0^{l_{max}} P(l)dl}{l_{max}} \tag{2.1}$$

where l_{max} is the maximum crushing distance of specimen before compaction zone and $P(l)$ is the area under the graph of load vs deformation.

Energy absorption can also be quantified in the form of specific energy absorption (SEA), which is the amount of absorbed energy per unit mass of crushed material and evaluated as in Eq. (2.2)

$$SEA = \frac{\int_0^{l_{max}} P(l)dl}{m} \tag{2.2}$$

where m is the mass of crushed specimen.

Crush force efficiency (CFE) compares the performance of specimen as a ration of the mean load to the peak load. Values closer or higher than unity are favourable, thus indicating a stable and progressive crushing process (Palanivelu et al., 2011). CFE is described in Eq (2.3) as:

$$CFE = \frac{P_{mean}}{P_{max}} \quad (2.3)$$

The ranking of parameters by decreasing priority in determining energy absorbing characteristics are specific energy absorption, mean load, peak load and lastly crush force efficiency. SEA is regarded as priority as it is normalised with the weight of specimen, giving an accurate measure of absorbed force per kilogram of specimen.

To test the static loading capacity of a specimen, it must undergo a quasi-static crushing test. This test involves the specimen placed in between two steel platens of a hydraulic press. The upper platen is then lowered typically at a low cross head speed, between 1mm/s and 20mm/s depending on the material crushed. Quasi static crushing/loading tests are commonly used to observe the behaviour of a sample in terms of axial compression. The crushing behaviour, coupled with the SEA value obtained, determines the failure mode as well as the suitability of the sample in handling that load (Sivagurunathan et al., 2018)

From the crushing test. A graph of load vs deformation/displacement will be obtained, as seen in Figure 2.1. The region after peak load is regarded as the post-crushing zone and is where most energy absorption parameters are observed. This region extends to the beginning of compaction zone as seen in Figure 2.1. By using the load vs displacement graph, Figure 2.2 shows the common failure modes experienced by composites (Kaneko et al., 2017). Development of peaks in the post-crushing region indicate progressive folding happening to the composite. A relatively stable load value after achieving peak load is a sign of progressive crushing in the composite specimen.

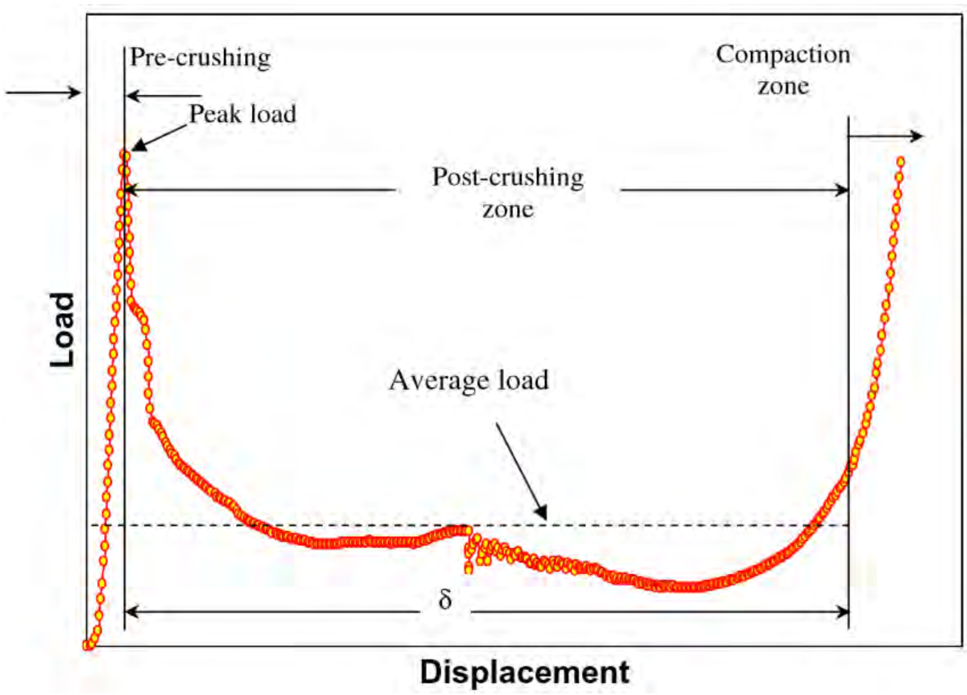

Figure 2.1: A typical load vs displacement graph of a quasi-static crushing test (Ataollahi et al., 2012)

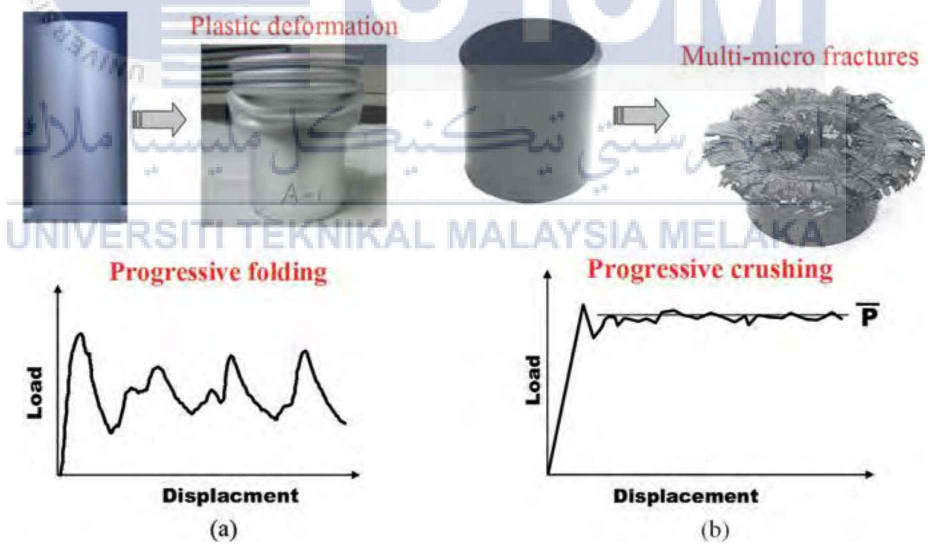

Figure 2.2: Examples of load vs displacement graph in a (a) progressive folding and (b) progressive crushing situation (Kaneko et al., 2017)

2.3 Fabrication Method

The application of composites has existed for over 500 years, dating back to time when Egyptians used mud and straw as composite construction blocks for added durability and strength. In the current age, there are many more advanced processes to fabricate composites, especially involving fibres as reinforcement. These new methods push the mechanical properties of composites to the maximum, where their mechanical properties can now rival that of metal.

2.3.1 Hand Lay-Up

One of the earlier methods that is still being used today is hand lay-up. This technique involves manual stacking of the fibre layers, while coating each stacked layer with the binding matrix. Once every layer is placed on the shaped mould, a roller is used to press the layer, as seen in Figure 2.3. This not only removes any trapped air bubbles between layers, but also ensures that the coating of binding matrix is even and uniform throughout the surface. Hand lay-up method is cheap, easy, and versatile in terms of shaping and forming the desired product. However, it requires large amounts of labour hours, especially for detailed or large-scale products (S. Y. Kim, Shim, Sturtevant, Kim, & Song, 2014).

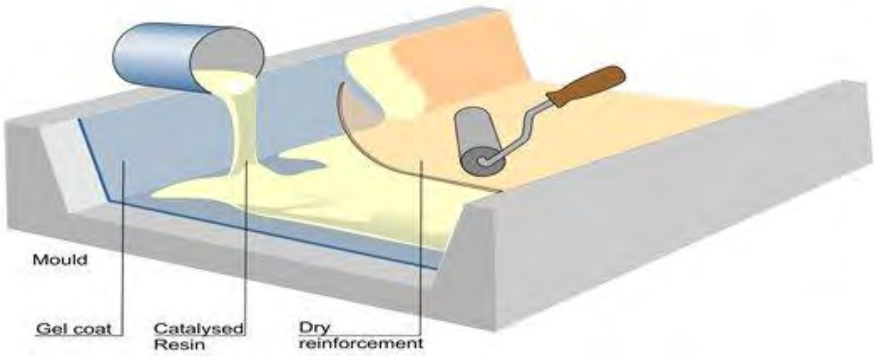

(a)

(b)

Figure 2.3: (a) Illustration of hand lay-up method and (b) demonstration of process (Gopal & Ramnath, 2016).

2.3.2 Bladder Assisted Prepreg Moulding

Bladder assisted moulding is a composite fabrication process that involves resin transfer moulding (RTM). This method starts by wrapping the thermoset pre-impregnated (prepreg) fibres around an inflatable bladder and placing it in the mould of desired shape. The mould is then placed in an autoclave oven to heat up and activate the impregnated resin in the fibre, allowing the fibre to be shaped (Figure 2.4). The bladder is then inflated to push on the inner wall of fibre. This forces the fibre to take on the shape of the mould and keep it in place as the composite is given time to set after removal from the autoclave. Inflatable bladders are also used to remove trapped air voids in between the layers of stacked fibres. The final product can be retrieved after the resin has fully cured, and the bladder is deflated (Anderson & Altan, 2016).

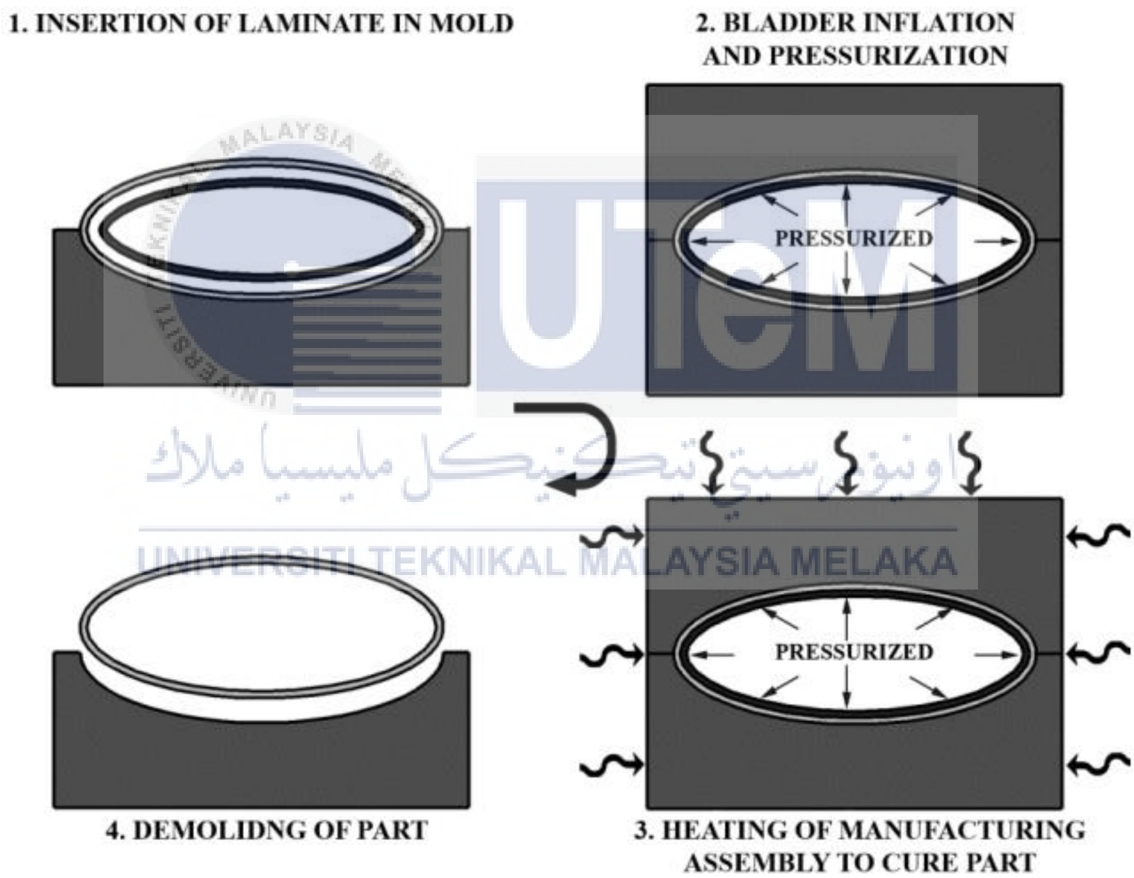

Figure 2.4: Process flow of bladder assisted composite manufacturing (Anderson & Altan, 2016)

One challenge that is commonly associated with this method is the presence of void content in the composite. This is because the bladders have to be inflated to pressures surpassing 5 bar (500 kPa) to effectively eliminate most of the void spaces between fibre layers (Anderson & Altan, 2016). Therefore, the mould must be able to contain the pressurized bladder without causing structural failure.

2.4 Factors that Affect Energy Absorption

Numerous factors can affect the energy absorption capabilities of fibre reinforced composites. Factors such as fibre stacking, triggering mechanism, fibre orientation and many more are extensively researched to determine the optimum fibre configuration and geometry of composites to be used in various applications.

2.4.1 Fibre Stacking

Fibre stacking involves the layering of the fibres in the composite during the lay-up process. The sequence of fibre lay-up (Figure 2.5) is determined through many factors, chief among which are type of fibres used (natural, synthetic, hybrid) and fibre orientation. This sequence has been proven to significantly diversify a composite's ability to sustain loading in an event of a crash. It is also worth noting that most of the studies mentioned stacked the fibre layers in symmetry, where the types of fibres are mirrored from the middle layer. This ensures that the deformation that occurs are the same throughout, especially for the inner and outer surfaces of the composites. (J. S. Kim, Yoon, & Shin, 2011)

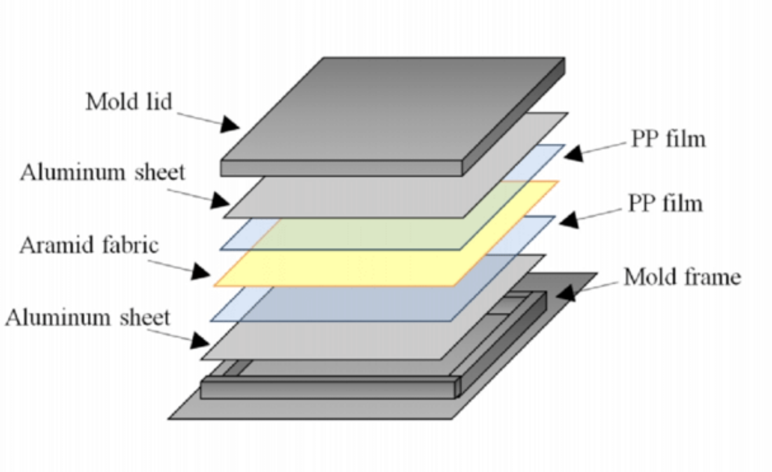

Figure 2.5: Example of fibre stacking sequence (Gonzalez-Canche, Flores-Johnson, & Carrillo, 2017)

An early attempt by Hitchen and Kemp (1995) investigated how the stacking sequence can affect the amount of impact sustained by carbon/toughened epoxy composite panels. Hitchen and Kemp fabricated composites with six layers of 0^{o} and 45^{o} fibres (equal numbers). All 6 possible fibre sequences were used to produce the composites. They found that the stacking sequence had significant effect on the crashworthiness of the composites, especially in terms of pre- and post-compression strengths. Composites that are layered in symmetry with 0^{o} fibres on the surface layers performed the best, due to its smaller delamination area after the impact.

One particular study by Hosseini and Shariati (2018) was done to determine the effects of using unidirectional, biaxial (90/0 and +45/-45) and tri-axial (+45/0/-45) oriented glass fibres to produce cylindrical epoxy composites and compare their energy absorption capabilities with unidirectional carbon/epoxy composites. Their comparative study found that composites that were produced from biaxial (90/0) oriented fibres produced the higher

SEA values. Moreover, those composites underwent uniform deformation, as observed in the splaying of fibres during the crushing process in Figure 2.6.

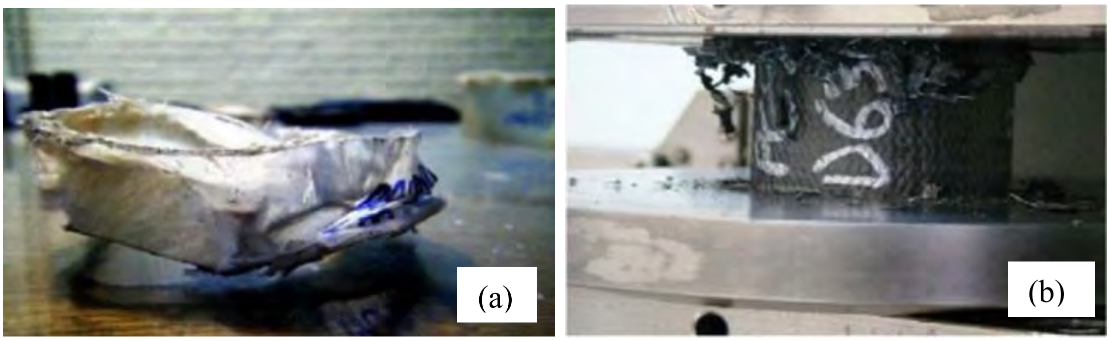

Figure 2.6: Crushing behaviour (a) triaxial (+45/0/-45) (b) biaxial (90/0) composites (Hosseini & Shariati, 2018)

When Abdullah et al. (2017) tested the quasi-static loading capabilities of woven kenaf/epoxy composites up to 4 layers, they found that P_{max} undergoes a 49.56% increase compared to 2 layered composites. The force versus displacement graph (Figure 2.7) shows that the two-layered composite specimens deformed in a stable manner throughout the test, whereas the four layered composites did not deform in a stable and uniform manner. This is due to the initial spike in P_{max} as seen in the graph. The SEA values however significantly increased as the multi-layered composites were tested, which bears the findings of Hosseini and Shariati (2018). They found that the SEA values increased for double layered composites when compared to single layered composites, as seen in Figure 2.7. Despite that, the values significantly dropped for the tri-axial (triple-layered) composites. Hosseini and Shariati suggest that this could have occurred due to asymmetrical stacking of fibre, or native properties of fibres itself that could have influenced energy absorbing behaviour during the crushing process.

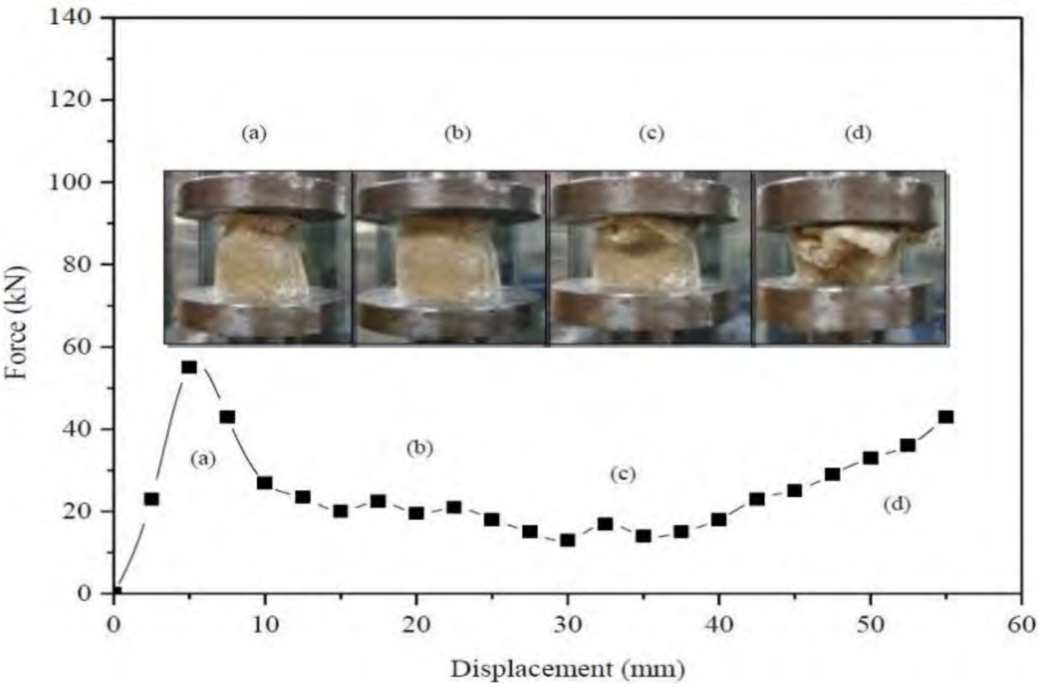

(a)

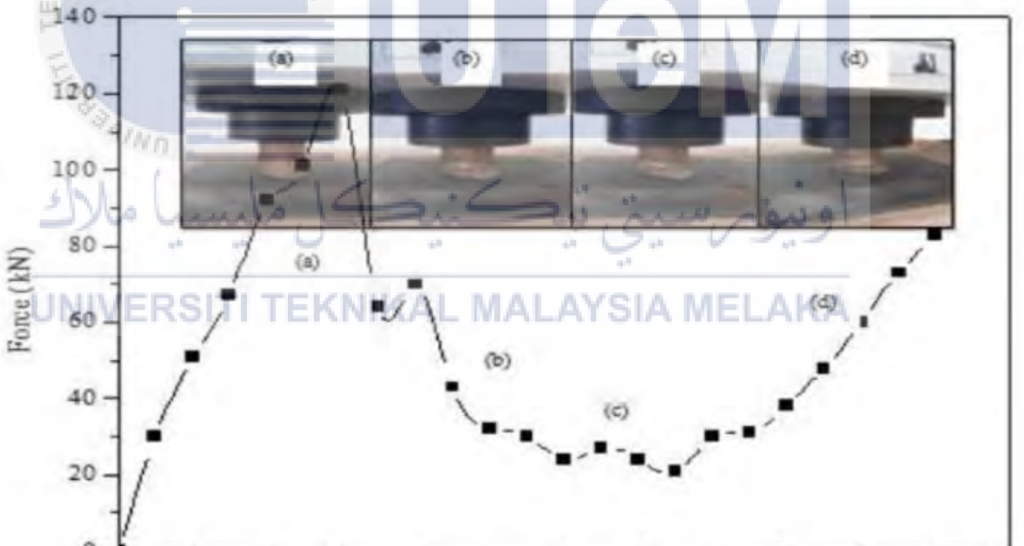

(b)

Figure 2.7: Crushing responses of (a) single layered and (b) double layered composite tubes (Abdullah & Ismail, 2017)

Another branch of fibre stacking explored were hybrid composites, where two or more types of fibres are sequentially stacked in a matrix bonded composite. In 2015, Sathish et al. performed tests to investigate the mechanical properties of hybrid composites made from a mix of unidirectional woven banana and kenaf fibre. Based on the results, it was recorded that the overall energy absorption was improved by applying hybrid sequencing. However, the performance of composites was also further improved by changing the fibre orientation and fibre content percentage while keeping the stacking sequence constant.

Sanjay and Yogesha (2016) tested hybrid jute and E-Glass fibres composites performance in an impact test. Composites with mixed stacking between Jute and E-Glass fibres were compared with composites made purely from either fibre. Interestingly, the composite made purely from E-Glass fibre achieved the highest impact strength, while the pure jute composite performed the worst (Figure 2.8). This study exhibits that symmetrical stacking of fibres does not necessarily improve the crashworthiness capabilities of composites tested. In Sanjay's research, symmetrically stacked composite specimens displayed identical deformations such as lamina bending and delamination in the outer and inner walls of the composites.

Composites	Compositions
L1	G + G + G + G + G + G + G + G + G + G
L2	J + J + G + G + G + J + J
L3	J + J + J + J + J + J
L4	G + G + J + J + J + J + G + G

(a)

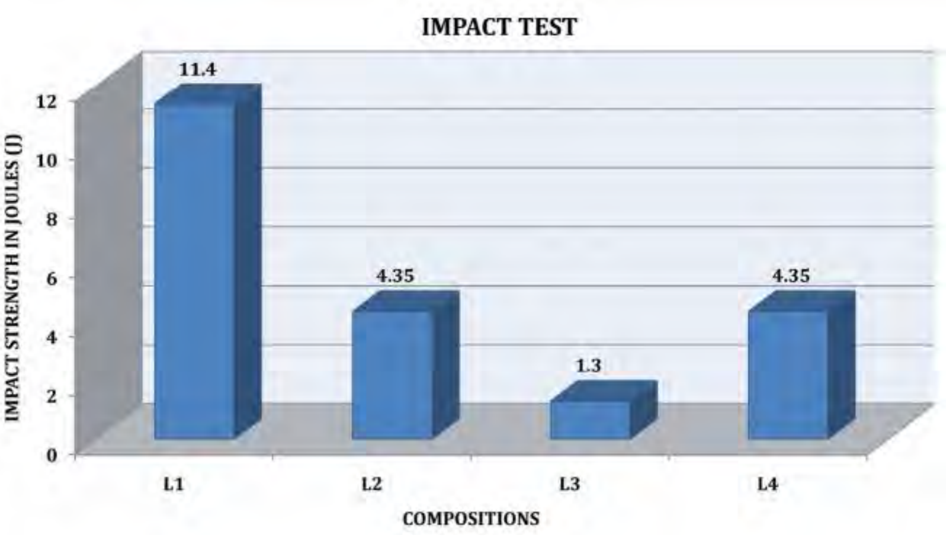

(b)

Figure 2.8: (a) Stacking sequence (G - Glass Fibre, J - Jute Fibre) of samples and (b) their subsequent impact strength (b) (Sanjay & Yogesha, 2016)

2.4.2 Trigger Mechanisms

A trigger mechanism in a solid body represents a specific point or region where the stress is localized. In the event of crushing or impact force, the failure of the body begins at the point of stress at the triggering mechanism, and then propagates through the rest of the body. Without a triggering mechanism, the crush test will result in the specimen having a high peak load (P_{max}) and low specific energy absorption value (SEA). A specimen that obtains a high peak load has shown to undergo abrupt and catastrophic failure. When experiencing a crash, the body will not be able to propagate and distribute the load in an even manner, therefore harming or damaging its contents/occupants (Courteau., 2011)

A significant amount of literature has been published on the influence of triggering mechanisms. These studies show that adding a triggering mechanism to a body will alter the energy absorption characteristics and other mechanical properties recorded in a quasi-static axial crushing test.

Siromani et al. (2014) investigated the effects of chamfered triggers and crush-cap triggers on the crashworthiness of unidirectional graphite/epoxy reinforced tubes. From the study, it was found that 45° chamfered ended composite tubes displayed the best progressive failure and uniform splaying of the fronds from the deformation as seen in Figure 2.9 The chamfered ended composites achieved an average peak load of 27kN, compared to crush-cap and flat ended specimens which achieved 39kN and 75kN respectively.

Sivagurunathan et al. (2018), studied the effects of internal triggers such as chamfered triggers and tulip triggers on woven jute/epoxy composite specimens compared to specimens with no trigger (flat ended). The quasi-static crushing test was performed at a cross-head speed of 10mm/min. The single and double chamfered ended specimens displayed higher average P_{max} values (32.97kN and 33.51kN respectively) compared to the flat-ended tubes (31.13kN). Figure 2.10 shows that single-chamfered specimens suffered catastrophic failure, unlike the axial cracks and fibre fractures that occurred in tulip triggered specimens.

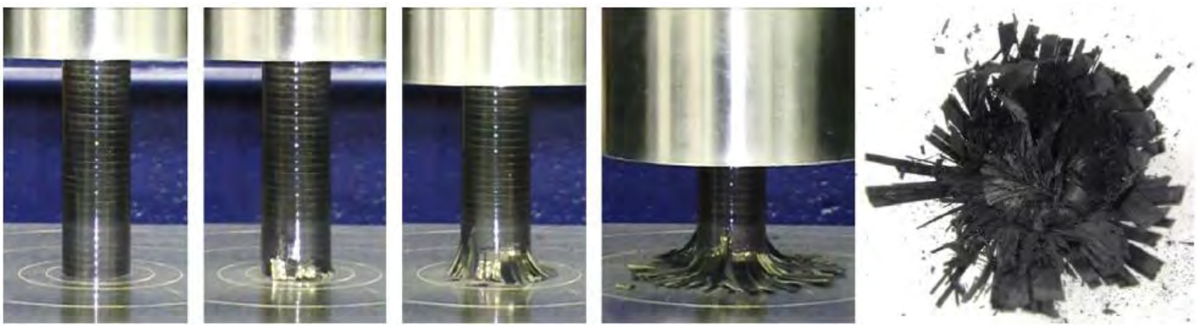

(a)

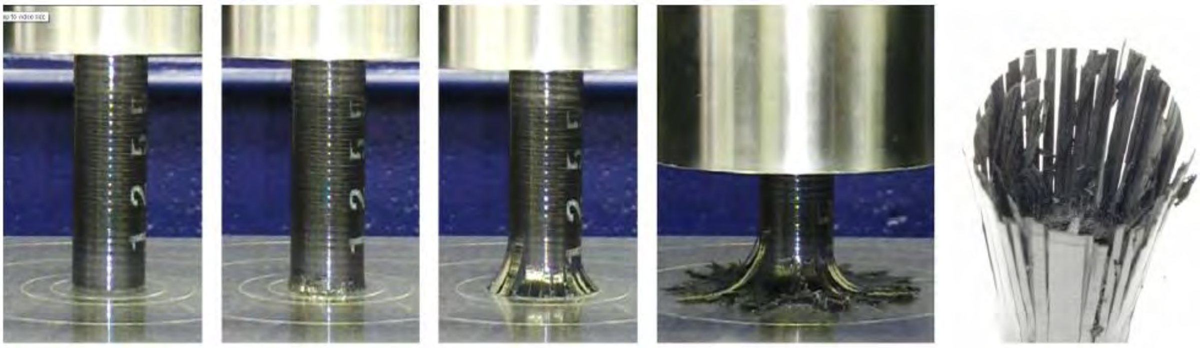

(b)

Figure 2.9: Crushing of (a) flat (b) chamfered ended composites at 0mm, 1.5mm, 10mm, 40mm and at final State (Siromani et al., 2014)

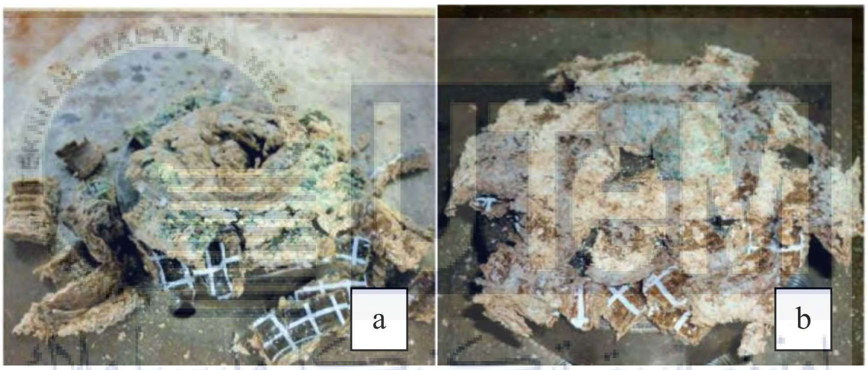

Figure 2.10: Comparison between (a) single chamfered and (b) tulip after crushing test (Sivagurunathan et al., 2018)

Research on the effectiveness of tulip triggers (Figure 2.11) was done by Chiu et al. in 2015 where they studied the effect of strain rate on the energy absorption values of tulip triggered unidirectional carbon/epoxy prepreg composites. Chiu et al. attempted to optimize the strain rate to get the highest value of SEA from the tested composites. From the results, the SEA values and P_{max} values did not differ significantly when the strain rate was increased. Specimens from both low and high strain rates were observed to have similar deformation characteristics (Figure 2.12).

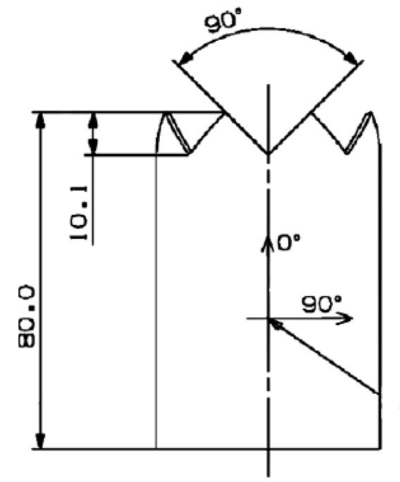

Figure 2.11: Tulip trigger dimensions and orientation (Chiu et al., 2015)

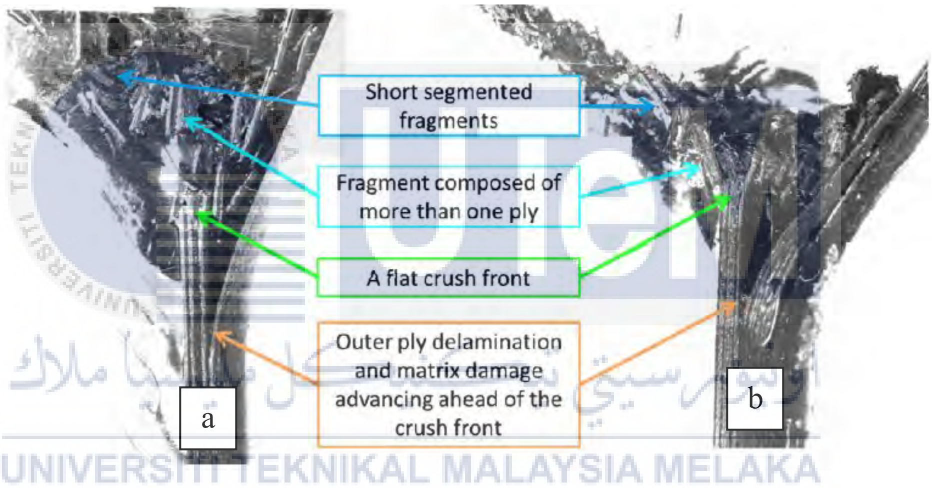

Figure 2.12: (a) Low strain rate vs (b) high strain rate displaying similar deformation (Chiu et al., 2015)

Aside from chamfered and tulip triggers, there are different types of triggers that are rarely researched. An experimentation was performed by Huang & Wang (2010) to determine the capability of ply drop-off and SMA (Shape Memory Alloy) triggers (Figure 2.13). It was observed that SMA triggers performed the best, with a 27.14% increase in average SEA value compared to flat-ended composites. The ply drop-off triggered composites achieved a 10.52% increase in average SEA value (Figure 2.14). It was also observed that composites of both types of triggers could efficiently initiate and remain in a stable/progressive failure mode throughout the quasi-static crushing test. Huang & Wang (2010) credited the increase in SEA values due to the constraint effect created by the triggers, which shorten the resulted laminar bundle length and achieving superior energy absorption characteristics.

Figure 2.13: Ply Drop Trigger (right) and SMA Trigger (left) (Huang & Wang, 2010)

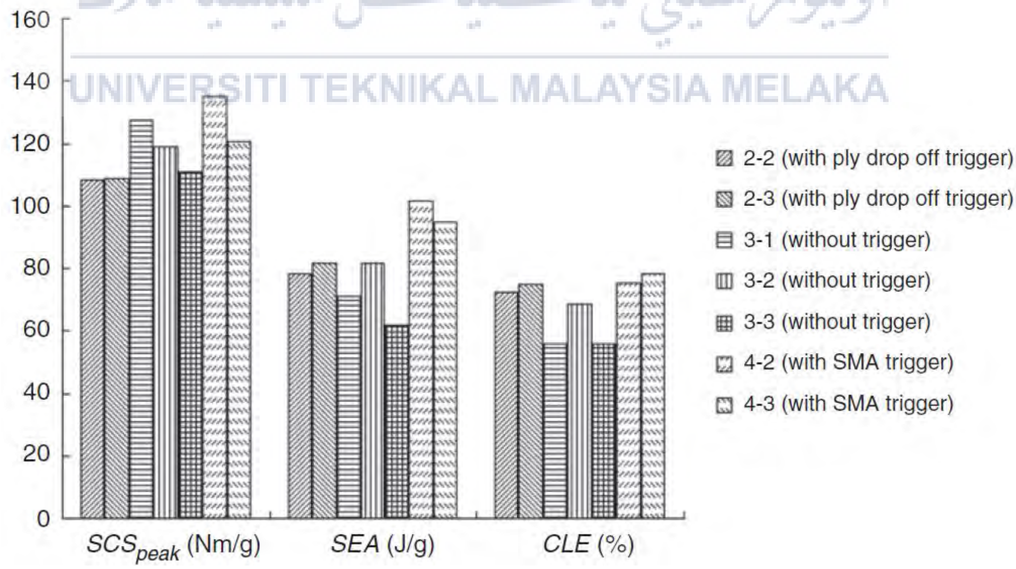

Figure 2.14: Comparison of Non-Trigger, Ply Drop Off, and SMA Trigger Performance (Huang & Wang, 2010)

Eshkoor et al. (2013) examined the effects of varied external triggering mechanisms on the crashworthiness characteristics of unidirectional oriented woven natural silk epoxy composite tubes. The research involved adding a plug-type trigger and a four-piece trigger (Figure 2.15) to the bottom platen of the crushing test machine. The plug trigger was determined to be a better external trigger, with a much lower P_{max} and higher SEA value compared to non-trigger and four-piece trigger specimens as seen in Figure 2.16. However, it displayed non-uniform deformation during the crushing test due to the contact point of the composite and the trigger mechanism on the lower platen.

Figure 2.15: (a) Plug and (b) 4-piece trigger

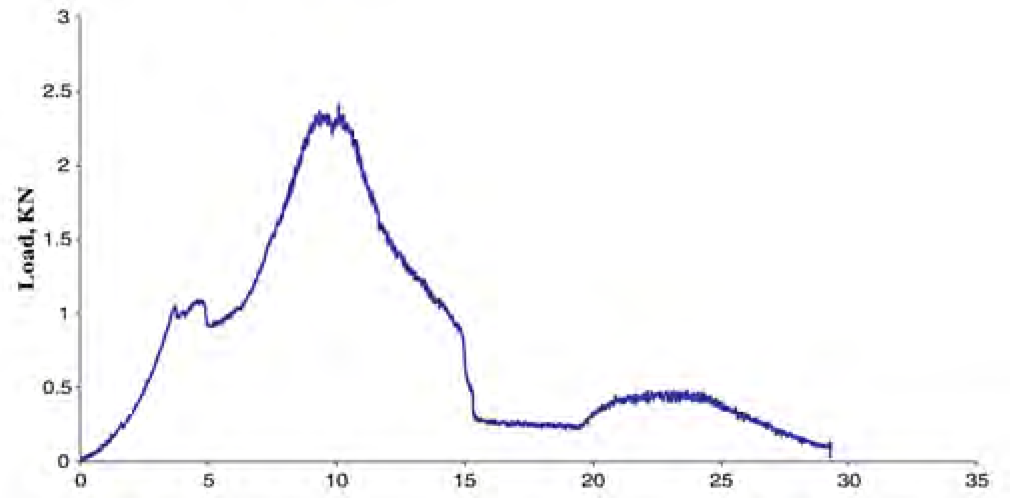

(a)

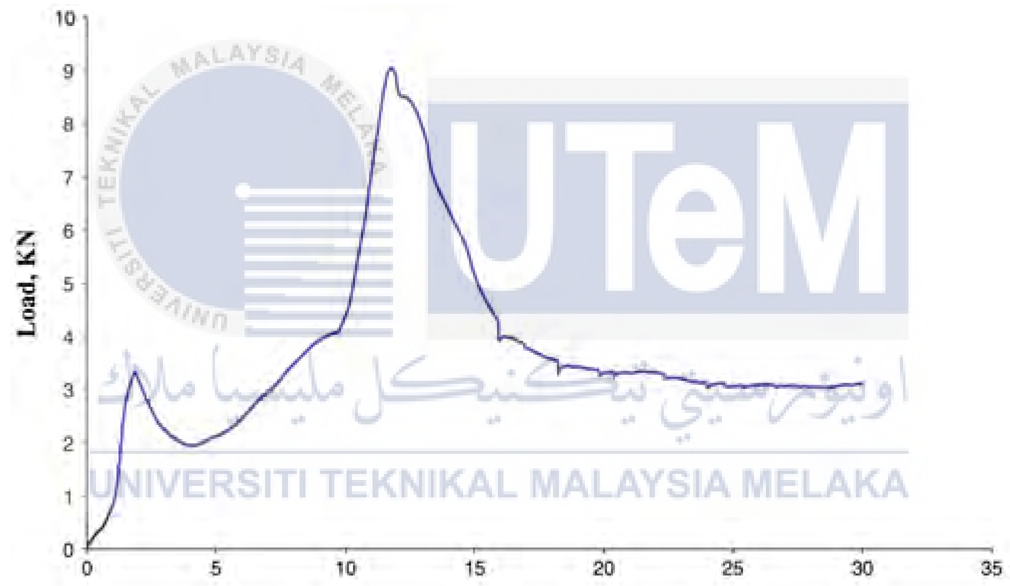

(b)

Figure 2.16: Results of (a) plug and (b) four-piece trigger crushing test (Eshkoor et al., 2013)

2.4.3 Fibre Orientation

The placement and orientation of fibre in any composite production method is crucial in determining its mechanical properties, especially crashworthiness and energy absorbing characteristics. The orientation angle (Figure 2.17) is determined during the fibre weaving process, either hand-made of machine woven. The orientation of fibre used depends largely on the final use of the fibre, and the type of loading it will be supporting. Isotropic composites are made with fibres that are independent of the direction of applied force, whereas anisotropic composites are produced with fibres that are unidirectional and dependent on the direction of applied force. One way to produce isotropic composites is to use fibres of varying orientation angle in a random manner, where the fibres are stacked without order of angle (Wang et al., 2016).

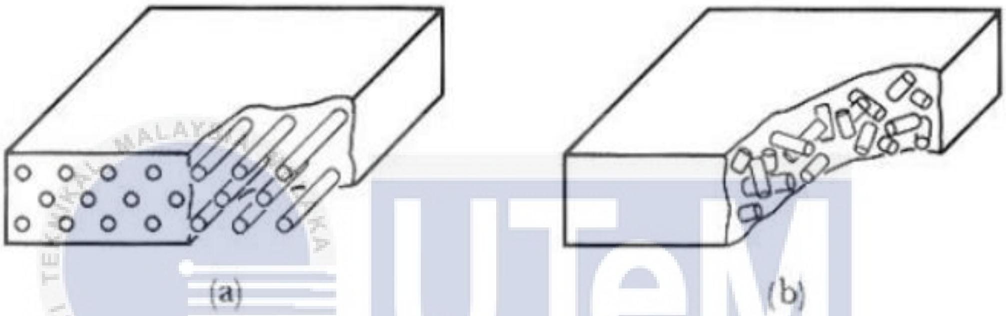

Figure 2.17: Internal structure of (a) unidirectional (b) random oriented fibres (Alhashmy, 2018)

Much of the current literature on fibre orientation in composites pays particular attention to the application of unidirectional fibres, whether for isotropic or anisotropic composites. A study by Hu et al. (2016) involved the relationship between increasing the fibre orientation angle in relation to the direction of applied loading and its effects on the P_{max} and SEA values obtained from a quasi-static axial crushing test. The specimens tested were woven glass cloth/epoxy composites with orientation angles 0°, 15°, 30°, 45°, 60° and 75°. As the value of theta was increased, it was reported that the specimens started deforming in catastrophic failure modes (Figure 2.18). Specimens with an orientation angle 60° and 75° underwent brittle fracturing crushing mode, as opposed to the lower theta value specimens that displayed lamina bending crushing mode (uniform splaying). The data obtained from the crushing tests support the observations, where the value of P_{max} decreases as the θ value is escalated. Moreover, the specimen with a θ value of 15° achieved the highest SEA value out of the other specimens (82.0 J/g).

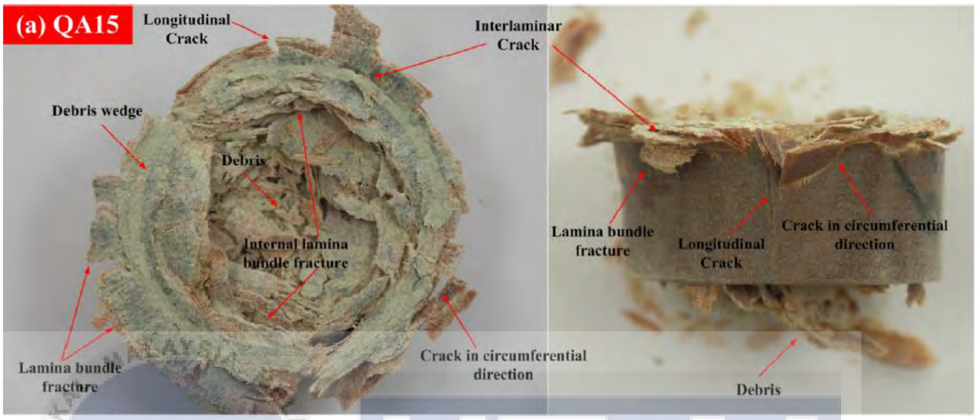

(a)

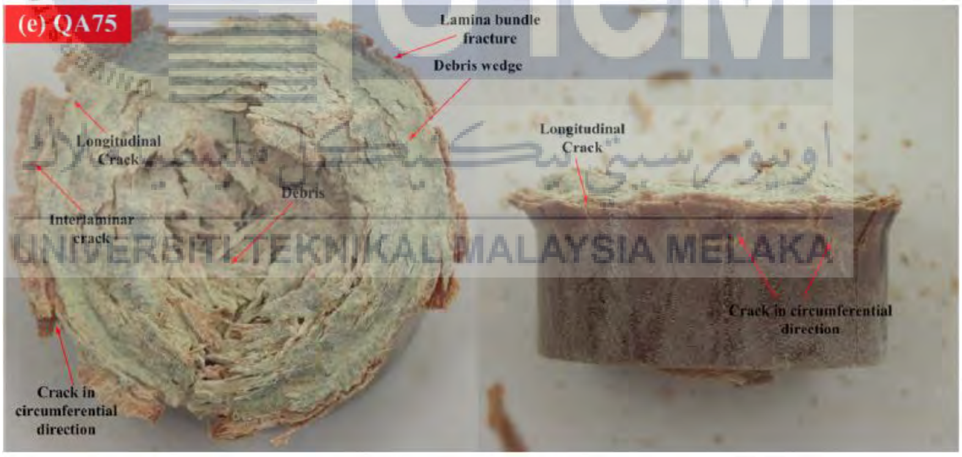

(b)

Figure 2.18: Post crushing analysis of (a) QA 15° (b) QA 75° fibre composites (Hu et al., 2016)

These findings are in line with the trend of data obtained by quasi-static crushing tests conducted by Wang et al. (2016) and Abdullah et al. (2017), where a decrease in P_{max} was observed as composites of increasing orientation angles were tested. In the case of Wang et al. (2016), the data showed a 9.92% decrease in P_{max} as the θ value was increased from 15° to 75° in the unidirectional carbon/epoxy composites. However, all three studies also observed that as the θ value of the fibre is increased, the SEA value significantly decreases (Figure 2.19). This indicated that fibres of high θ values are non-uniformly distributing the applied forces after the initial peak load, therefore resulting in the inability of the specimen to absorb energy efficiently.

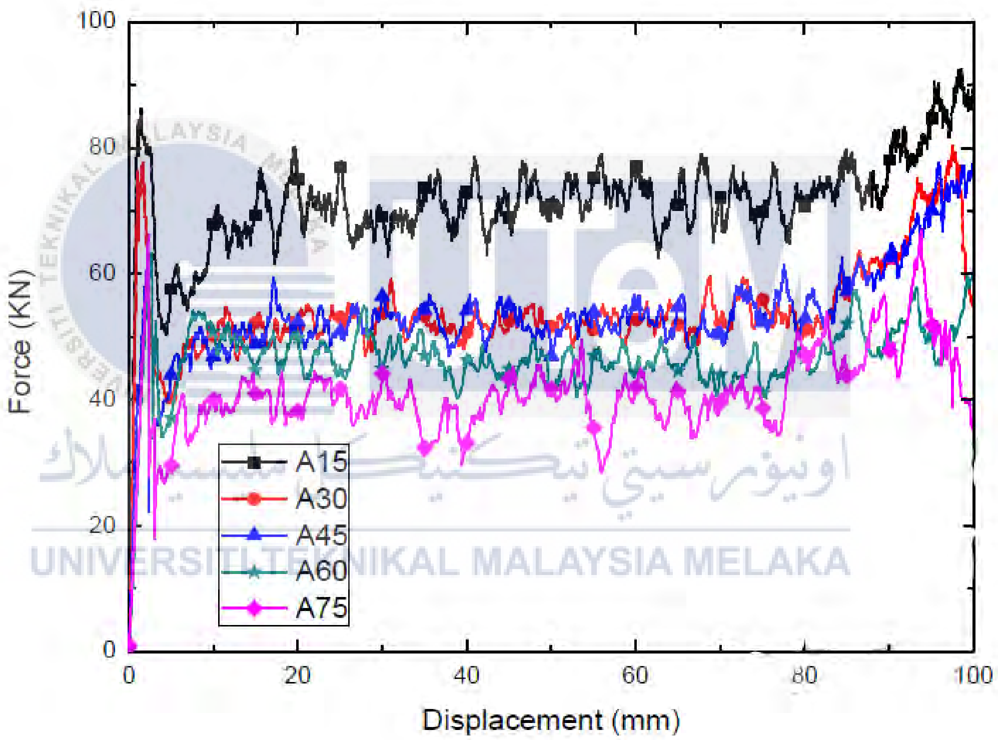

Figure 2.19: Force vs displacement for quasi-static crushing with different thickness (Wang et al., 2016)

2.4.4 Geometrical Parameters

This characteristic involves the diameter, thickness, length and other measurement constraints and how changing these values will affect the energy absorbing abilities of the composites. One of the more researched areas in terms of geometrical constraints is the ratio between inner diameter and thickness (D/t). Not only does this ratio determine the classification of composite tubes as thick or thin cylinders, but also highly influence the crashworthiness capability of the specimens.

A particular study conducted by Alia et al. (2014) examined the significance of increasing the D/t ratio in altering the mechanical properties of foam filled carbon fibre composites. Based on the crushing test results, it was detected that enlarging the D/t ratio caused the SEA values to steadily decrease in a proportionate manner (Figure XXX). In another analysis Pickett and Dayal (2012) performed a numerical study on the effects of scaling the D/t ratio of glass/epoxy tubes on its mechanical and crashworthiness properties. From their study, it was found that the decrease in the D/t ratio of the composites caused the SEA values to increase, and ultimately increasing the sustained crushing load (Table 2.1), similar to the findings of Alia et al. (2014).

Table 2.1: D/t Values and Corresponding SEA Values Obtained (Alia et al., 2014)

Test ID	D/t	Mass (g)	SEA (kJ/kg)
TCF10	6.3	0.95	93.3
TCF12	7.4	1.50	89.2
TCF29	16.9	3.90	81.4
TCF40	22.4	5.20	76.7
TCF50	28.0	6.50	58.5
TCF63	32.6	9.90	48.1

Both Alia et al. and Pickett et al. attribute the transition of SEA values to the interlaminar cracking in the crushed region of the tube. As the D/t ratio is decrease, the reduction of interlaminar cracking will also cause the buckling load of the specific laminar bundles to increase. Interlaminar delamination most commonly occurs due to the inherent characteristic of the matrix material to be brittle. Recently, a study by Zheng et al. (2017) further investigated the interlaminar delamination phenomenon in crushed composites and proposed an improvement to further reduce its effects on the energy absorption capabilities. It was found that inserting carbon nanotubes/polysulfone nanofibre (CNTs/PSF) paper between the layers of stacked fibre improved the interlaminar fracture toughness of the composites. The composites with CNTs/PSF interleafs displayed higher flexural strength (increase of 27%) compared to the control sample. Figure 2.20 shows the SEM pictures obtained after the test.

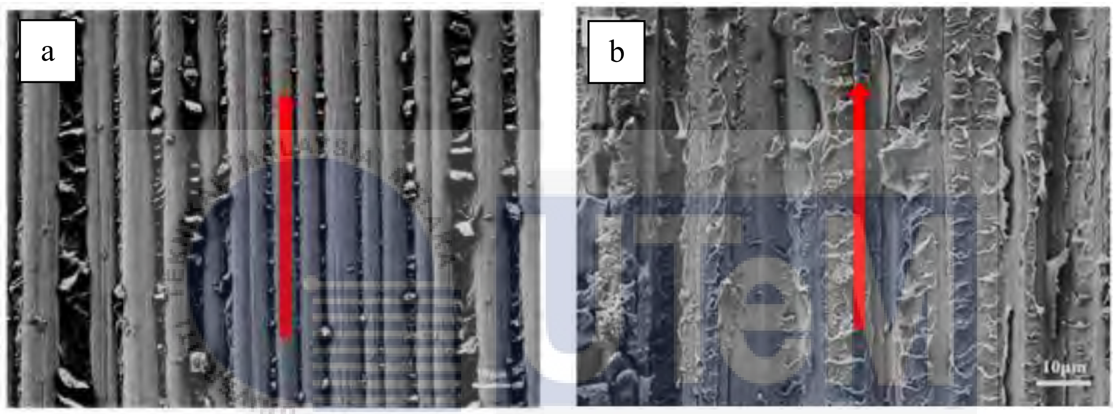

Figure 2.20: SEM surface laminate photos of non-reinforced vs CNTS/PSF interleafed composites (red arrow indicates crack growth)

2.5 Crushing Speed and Range

The crushing speed for this research was set at 10mm/min after observing a similar range of testing speeds in other studies. In many studies, the range of crushing speed is between 1mm/min to 20mm/min, suggesting that this is the quasi-static deformation range for composites that is being tested. In their 2012 study, Meredith et al. set the crushing speed to 1 mm/min in order to test the energy absorption capabilities of natural fibre composites. The similar speed was chosen by Alia et al. to assess the performance of foam filled carbon fibre epoxy composites.

A crushing speed of 5mm/min was chosen by Jackson et al. in 2011 to investigate open carbon fibre-epoxy composites. Interestingly, many studies set the value of crushing speed to 10 mm/min, including Palanivelu et al., Sivagurunathan et al., as well as Wang et al. in obtaining the data for the quasi-static crushing test. Eshkoor et al. configured the test to run at 20 mm/min to determine the crashworthiness of natural silk epoxy square tubes.

2.6 Summary

Based on the literature studied, findings can be summarized into several key points. Firstly, fibre lay-up sequence affects the energy absorption capabilities by introducing fibres of different mechanical properties that can alter how the composite deforms when introduced to load. Moreover, these studies also show that triggering mechanism of the specimen can modify the crashworthiness parameters of composites. This is mainly due to the triggers changing the initiation of load on the composite, as well as encouraging progressive crushing.

CHAPTER 3

METHODOLOGY

3.1 Introduction

This chapter details the methods, processes, as well as the procedures involved to conduct this research. The methodology is separated into two sections, fabrication and testing. The first section involves the fabrication process for the hollow composite cylindrical tubes through bladder assisted moulding process. Composites of different lay-up sequences will be produced. The composite tubes will be machined with varying triggering mechanisms (flat, 45° chamfers and tulip). The second part of the chapter focuses on the testing procedures to study the energy absorbing capabilities of the fabricated composites with different triggering mechanisms and stacking sequence. Figure 3.1 elucidates the research flow chart.

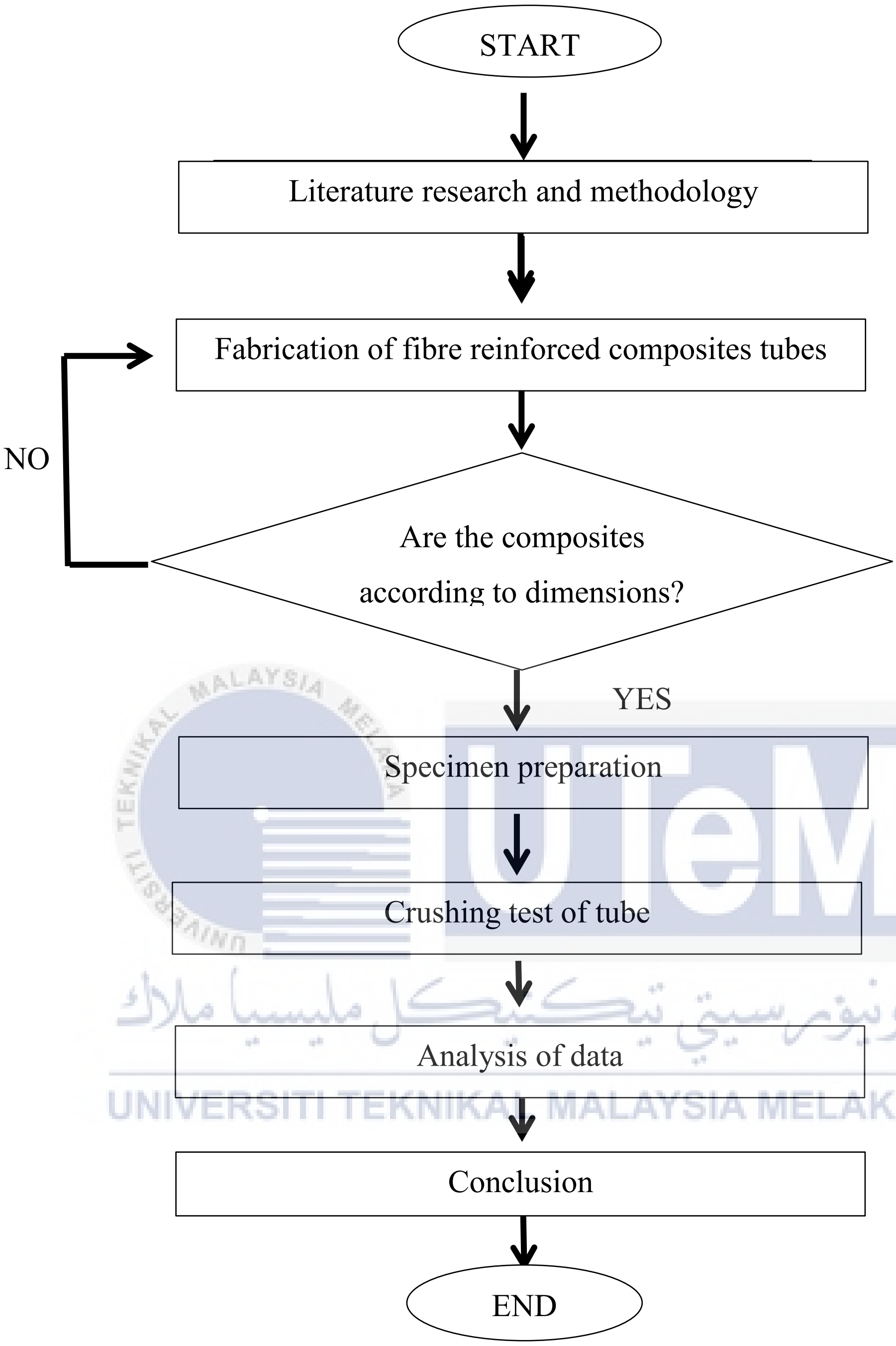

Figure 3.1: Flowchart of research methodology

3.2 Materials

This section details the materials used in fabricating the fibre reinforced composites.

3.2.1 Fibre

Two types of fibres (Figure 3.2) were used in the fabrication of composites. Uniform cross-ply 0°/90° glass fibre was used as the synthetic element in composites. The glass fibres (G) were supplied by ZKK Sdn. Bhd., Malaysia and is rated at 600 grams per square meter. Unidirectional banana fibre (B) was chosen as the natural reinforcing element in the composites. This fibre was manufactured at 225 grams per square meter, and supplied by J.C. Overseas Incorporation, India.

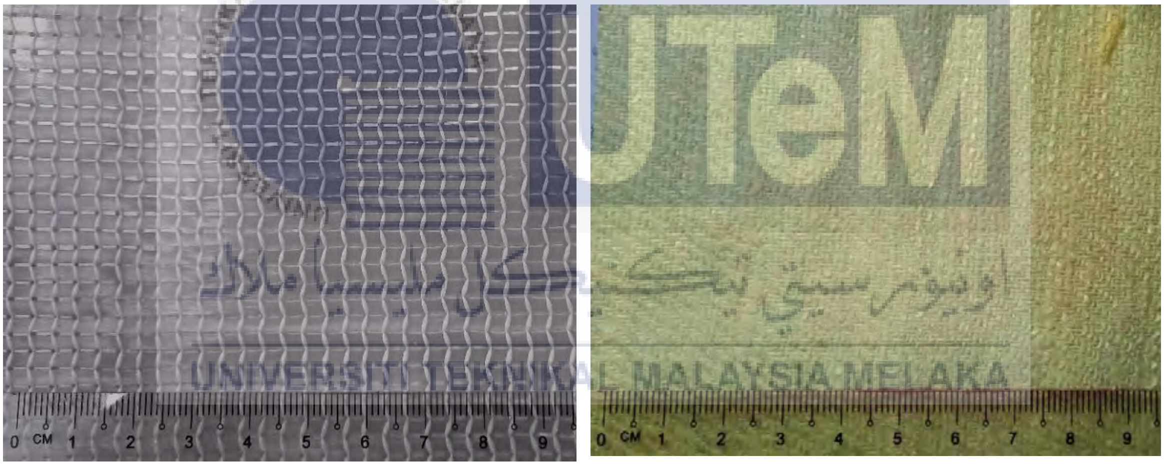

(a) (b)

Figure 3.2: (a) Uniform cross-ply glass fibre and (b) Unidirectional banana fibre

The ratio of banana fibre to glass fibre in terms of grams per square meter is approximately 1:3. Moreover, the fibre orientation of banana fibre is unidirectional, as opposed to the uniform cross-ply orientation of glass fibre. Therefore, each layer of glass fibre was represented with 3 layers of banana fibre to equalise the weight ratio. The 3 layers of banana fibres were placed in alternating angles of 0°/90°/0° to replicate the uniform cross-ply pattern.

3.2.2 Epoxy

The binding matrix used in this study is the Autofix 1710-A epoxy adhesive coupled with the Autofix 1345-B hardener (Figure 3.3). The matrix was supplied by Chemibond Enterprise Sdn. Bhd, Malaysia and is mixed in a ratio of 1:1. When mixed, it produces a clear and transparent product which takes 24 to 48 hours to fully cure. During the curing process, this epoxy will reach a maximum exothermic reaction of 70^{o}C.

Figure 3.3: (a) Auto-Fix 1710-A Epoxy and (b) 1345-B Hardener

3.3 Fabrication Process

Figure 3.4 shows the flow of fabricating the composite tube.

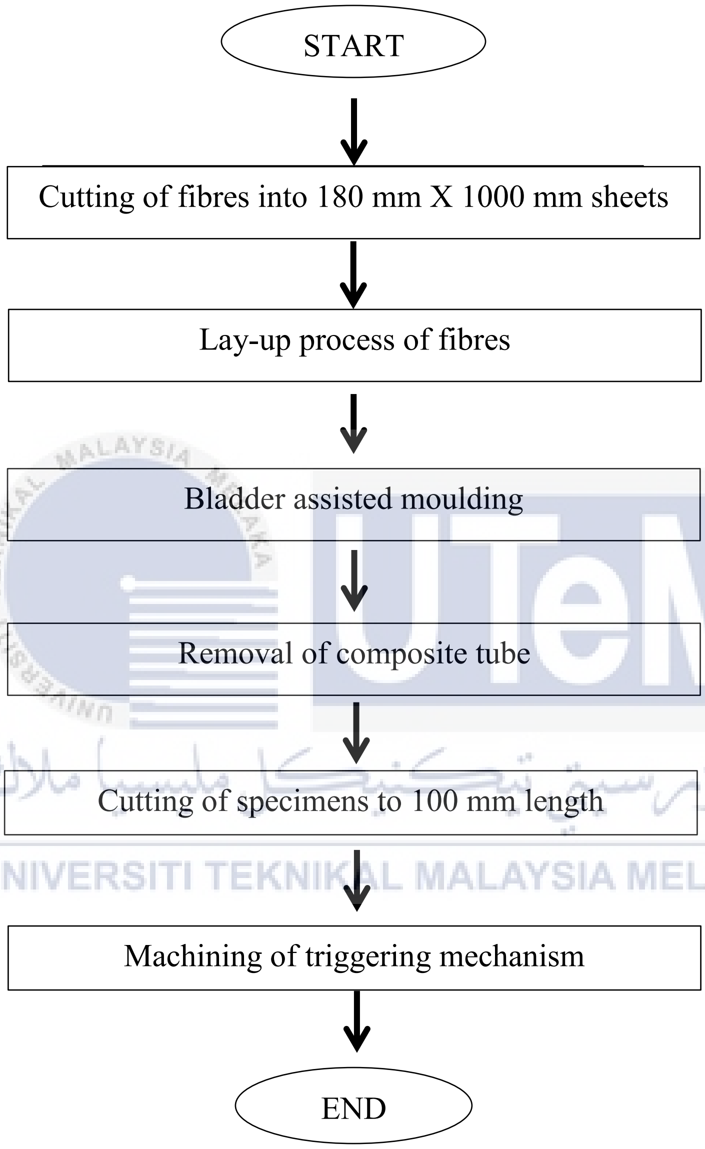

Figure 3.4: Flowchart of fabrication process

The lay-up sequences as seen in Figure 3.5 was done with four symmetrical sequences, that were GGG (all glass fibre), GBG (glass-banana-glass fibre), BGB (banana-glass-banana fibre) and BBB (all banana fibre). As the GSM (grams per square meter) ratio of banana fibre to glass fibre is 1:3, each layer of banana fibre is equalized by 3 layers of banana fibre layered in 0°/90°/0° positions. Epoxy will be applied on to each layer of fibre and stacked according to sequence.

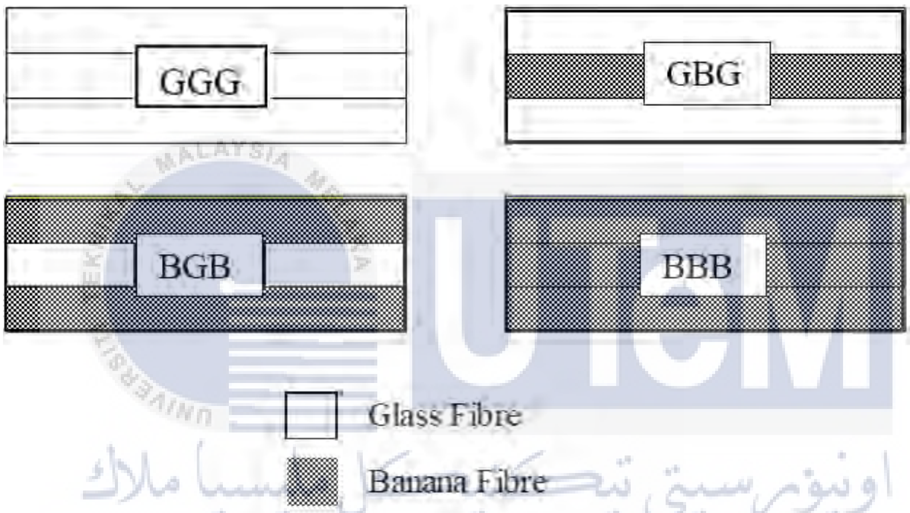

Figure 3.5: Fibre lay-up sequences of composites

To fabricate the composite tubes, the bladder assisted moulding method was applied. This involves using an inflatable bladder to push the fibres to the shape of the mould (Figure 3.6). A mild-steel pipe with a thickness of 3 mm was split in half lengthwise to create the cylindrical mould.

3.7.

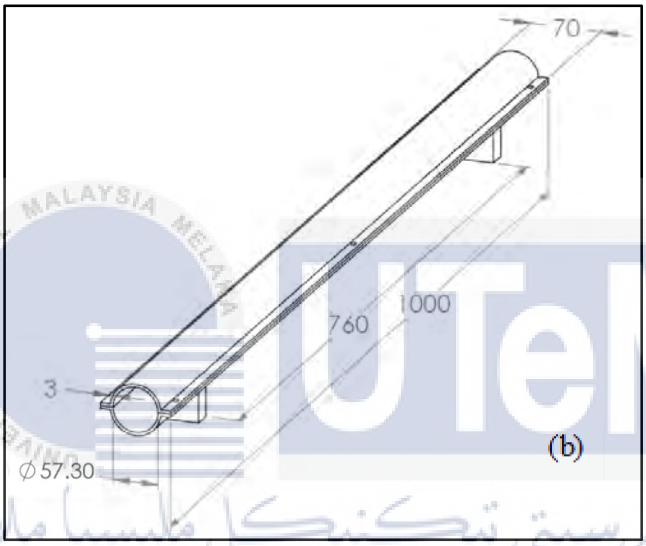

Figure 3.6: (a) Mould used for specimen fabrication and (b) dimensions of mould in mm

The bladder pressure was kept constant at 4 MPa until the composite cured fully (24 to 48 hours). The completed 1m long tubes will be removed from the mould and left to set for 72 hours. The tubes were cut into lengths of 100 mm by using the conventional lathe machine. Specimens with flat and 45° chamfer triggers were fabricated using the same lathe machine, while 4-petal tulip triggers were made with a table saw to evenly cut out the petals. The dimensions of triggers fabricated onto the composite specimens are detailed in Figure 3.7.

Each specimen was measured and weighed prior to performing the quasi-static crushing test. The measurements (length, thickness) was used to determine and analyse the variations in geometry in specimens. Thickness values of the specimens were taken at three locations, and an average value was determined. Weighing the specimen will allow the calculation of the Specific Energy Absorption.

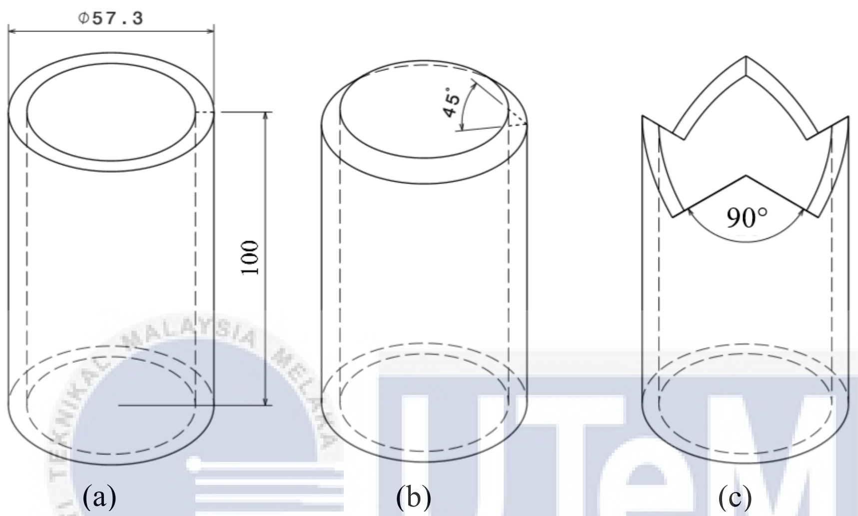

Figure 3.7: Dimensions of triggers on composites (a) flat-end, (b) 45° chamfer, (c) tulip

3.4 Testing Method

A quasi-static axial compression test is performed on the composites to determine their energy absorbing capabilities. Composites were placed between the platen and crushed axially using universal testing machine (UTM), Instron Model 5585 with 150 kN load cell. Based on literature research, the crushing rate for this test was set at 10mm/min at a stroke length of 85 mm (85% of crushing process), just as specimens enter the compaction zone.

The test starts at the point of contact between platen and composite, then continues past the densification of the specimen. The crushing process was photographed at certain stages to observe and record the deformation pattern of the composites. These photographs will be noted in the graph to indicate the failure mode at significant stages of the graph.

Figure 3.8: Universal testing machine Instron Model 5585

CHAPTER 4

DATA AND RESULTS

4.1 Introduction

This chapter focuses on the results of the quasi-static crushing test performed on the composite fibre tubes. Raw data obtained from the Instron 5585 machine will be used to determine the peak load, mean load, specific energy absorption and the crush force efficiency of the specimens. The first part of the analysis will compare the energy absorption characteristics of specimens with different triggering mechanisms within the same fibre lay-up sequence. This will be followed by the analysis of performance based on the fibre lay-up sequence of the specimens, and how it effects the energy absorption characteristics of the specimen.

4.2 Physical properties of Specimens

A total of 36 specimens were fabricated, with four different fibre lay-up sequences. Specimens from each lay-up were split into three varying trigger mechanisms, which are the flat-ended, 45° chamfer trigger, and the tulip trigger configurations (Figure 4.1). Appendix A gives the weight and the average thickness for each specimen.

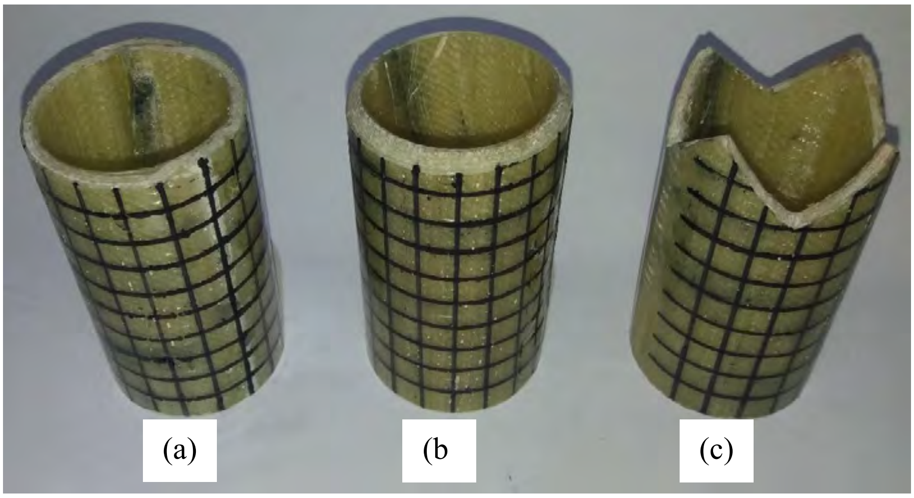

Figure 4.1: (a) Flat-ended, (b) 45° chamfer triggered and (c) tulip-triggered specimens of GBG lay-up

4.3 Quasi-Static Crushing behaviour

This section observes the sequence of photographs during the quasi-static crushing process, which is then cross-referenced with the load versus deformation graph. This will depict the energy absorption behaviour of the specimen. Photographs of crushing sequence also reveal specific occurrences that could further detail the characteristics of fibre reinforced composites.

4.3.1 GGG Lay-up Specimens

For the flat-ended fibre glass specimen, the specimen undergoes a critical drop in load after a peak load was achieved. This signifies that the specimen has failed to sustain the load, thus rapidly entering the plastic range of deformation as seen in the load vs deformation graph of Figure 4.2 (Siromani et.al., 2013: Luo et. al., 2016). In the post-crushing zone (between peak load and compaction zone), the specimen starts to delaminate and split into different segments as the crushing progressed. Fibre fracture seen in the end results of Figure 4.2 indicates that the specimen was able to sustain the load. The graph supplements this behaviour by denoting stable load values in the post-crushing zone.

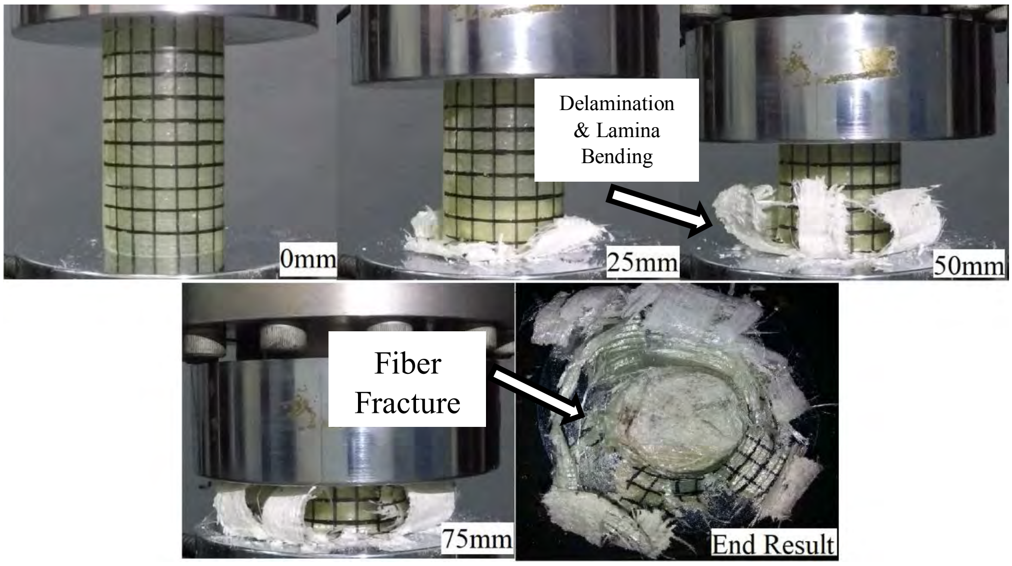

(a)

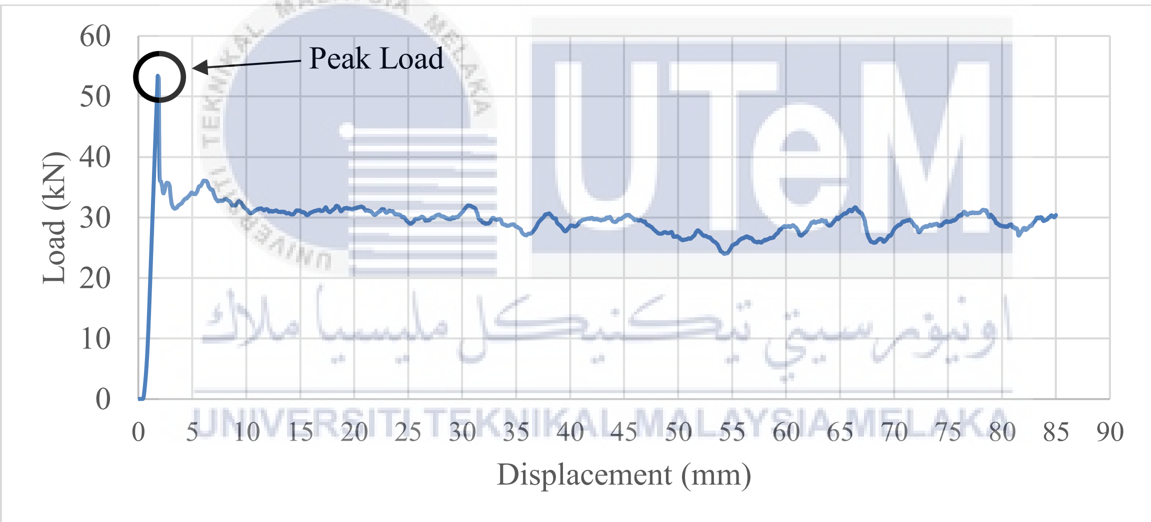

(b)

Figure 4.2: Quasi static compression test for flat-ended glass fibre tubes, (a) Photographs of specimen crushing at various stages and end result, (b) Load versus displacement during the crushing process.

For the chamfered GGG specimen, Figure 4.3 shows that it was able to reduce the peak load of the specimen, as well as reaching it later in the deformation compared to the flat-ended GGG specimen. This observation reveals the effectiveness of the chamfer trigger in energy absorption. Moreover, a transverse failure occurred early in the crushing process, which indicates that the specimen failed to sustain the load after reaching its peak load. The presence of long axial cracks in the end result of Figure XXX suggests that the specimen slowly lost its load bearing capacity as the crushing progressed (Palanivelu et al., 2011)

(a)

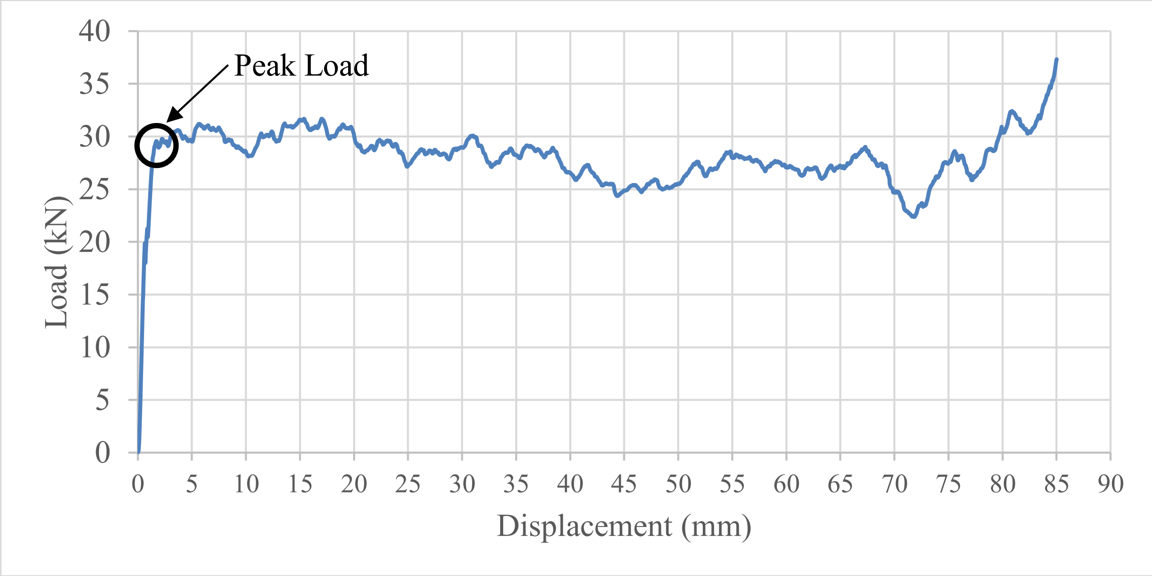

(b)

Figure 4.3: Quasi static compression test for chamfered glass fibre tubes, (a) Photographs of specimen crushing at various stages and end result, (b) Load versus displacement during the crushing process.

In Figure 4.4, the peak load is the lowest and occurred the latest at around 21mm of displacement, when compared to the earlier GGG specimens. In Fig 4.4 (a), lamina bending is observed as the load platen crushes the tulip triggers. This is evidence of progressive crushing as the tulip triggers evenly propagated the force, while having lower stiffness in a smaller impact surface (J. Huang & Wang, 2010). The lamina bending and delamination is continuously observed as the crushing process progressed. The end result shows no axial cracks, while displaying fibre fractures as the specimen enters the compaction zone. This suggests that the tulip trigger exhibited fair energy absorption capabilities as the presence of axial cracks indicate gradual failure of specimen.

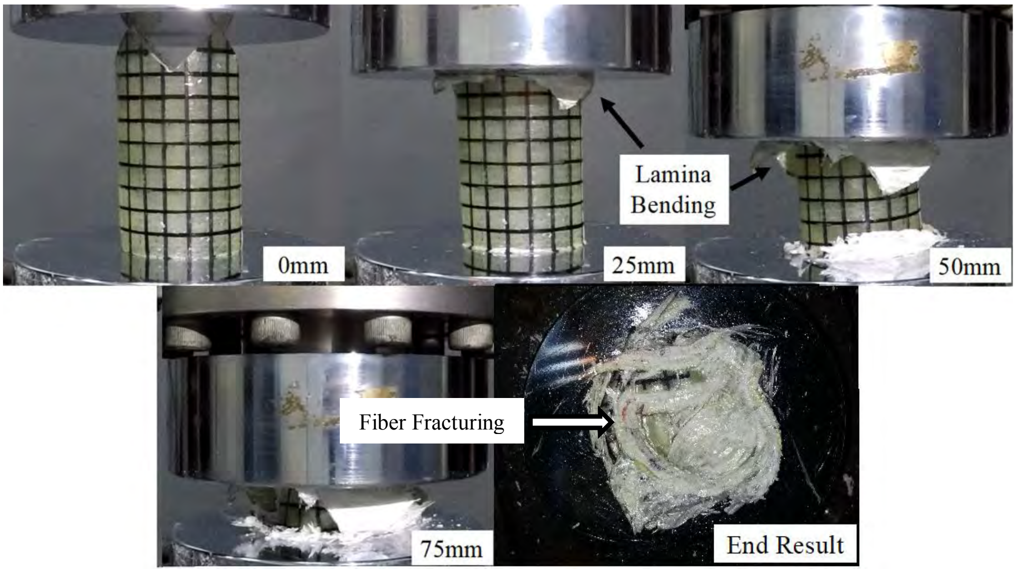

(a)

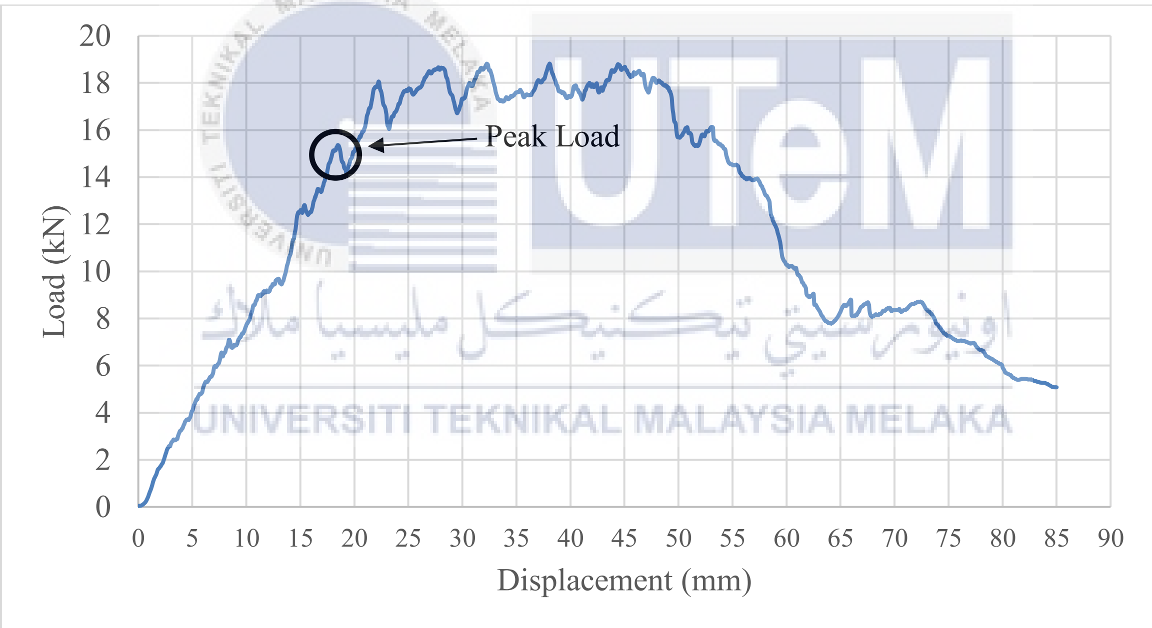

(b)

Figure 4.4: Quasi static compression test for tulip triggered glass fibre tube, (a) Photographs of specimen crushing at various stages and end result, (b) Load versus displacement during the crushing process.

4.3.2 GBG Lay-up Specimens

The flat-ended GBG specimen displayed similar characteristics as the flat-ended GGG specimen, where it reached the peak load early in the crushing process as seen in Fig 4.5. Delamination that developed after the peak load shows that the layers of different fibre in the specimen started to split after critical load bearing failure as observed in Fig 4.5 (b). The presence of delamination also provides evidence of efficient propagation of force within the layers of fibre. Axial cracks also began to form after 50mm of crushing distance. Towards the end of the test, transverse failure took place in the bottom region of the specimen, which is seen as a decrease load between the 60 and 70mm extension region of Fig 4.5 (b). Both axial cracks and transverse failure contribute to the broken off piece seen in the end result of Fig 4.5 (a).

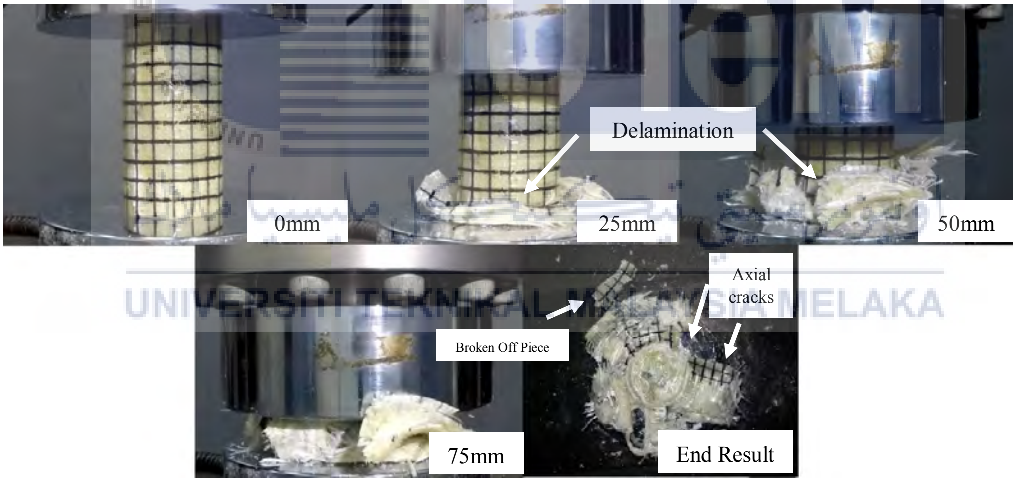

(a)

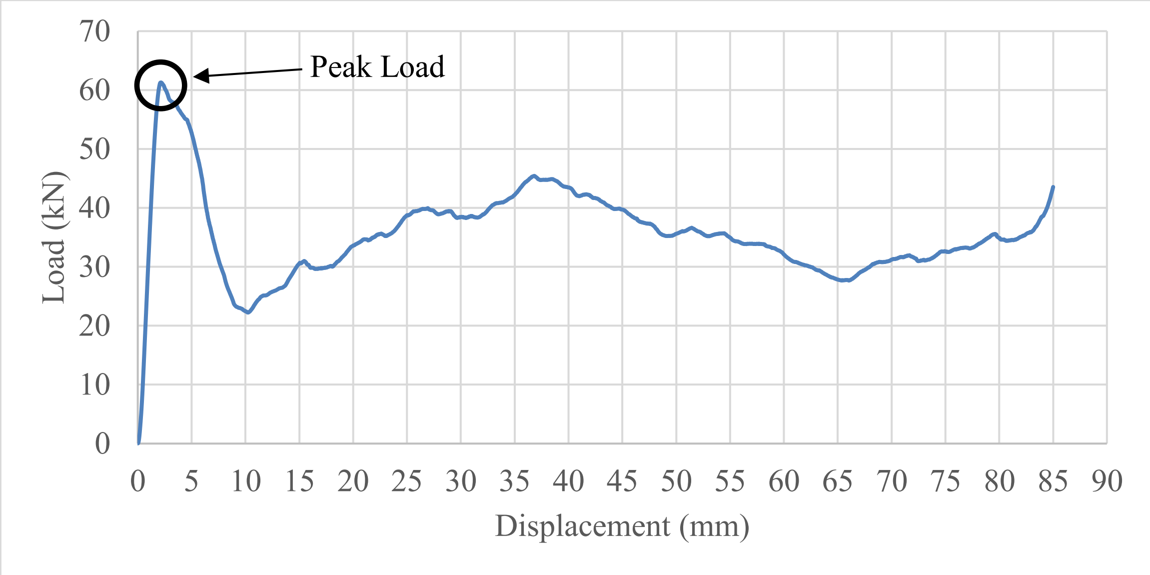

(b)

Figure 4.5: Quasi static compression test for flat-ended GBG tube, (a) Photographs of specimen crushing at various stages and end result, (b) Load versus displacement during the crushing process.

Figure 4.6 presents the crushing behaviour of the chamfered GBG specimen and its load vs displacement graph. As seen in the GGG samples, the peak load is attained at a later stage of crushing compared to the flat-ended sample due to the presence of a 45° chamfer. The progressive crushing and lamina bending observed until around mid-crushing process led to the increase of load in Fig 4.6 (b) from 10mm to 50mm of specimen extension. However, the appearance and spreading of axial cracks after 50mm extension caused the load bearing capacity of the specimen to gradually decrease over time, until the compaction zone was entered.

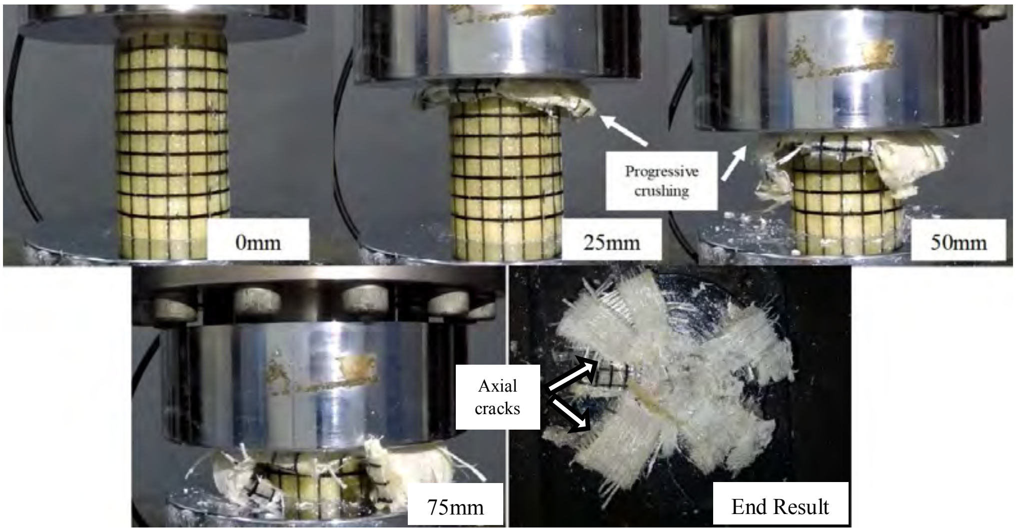

(a)

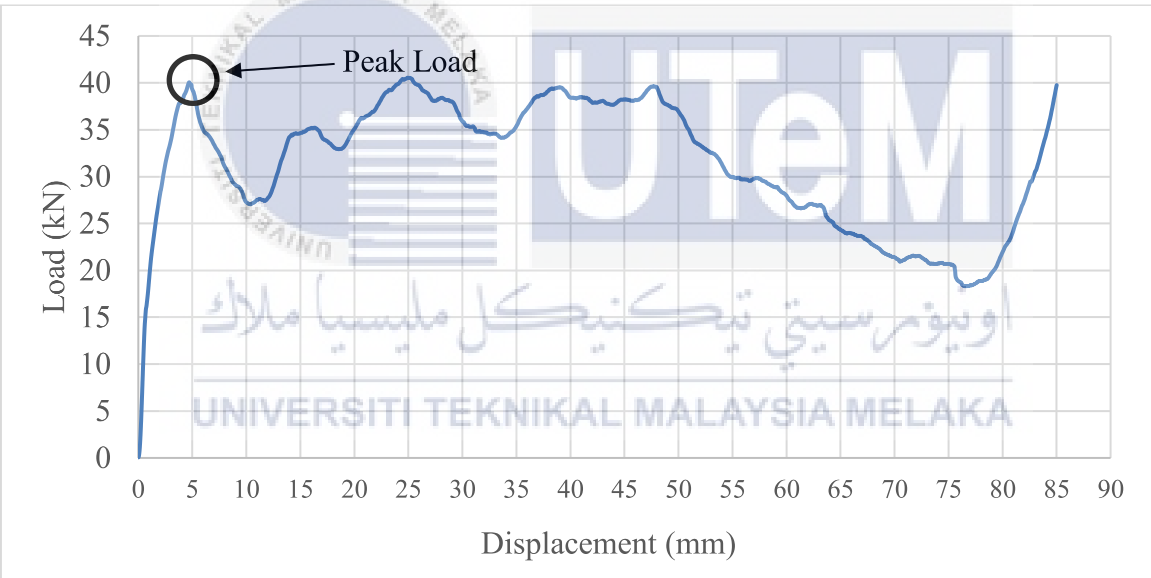

(b)

Figure 4.6: Quasi static compression test for chamfered GBG tube, (a) Photographs of specimen crushing at various stages and end result, (b) Load versus displacement during the crushing process.

In Figure 4.7, the crushing behaviour of one out three tulip-triggered GBG specimens is observed. The peak load is achieved later, at around 25mm of crushing distance. This is evidence that the tulip trigger delays and decreases the peak load due to the increased length of trigger zone that spreads the sudden load increase in the initial stage of crushing (Chiu et al., 2015). The tulip trigger also causes progressive crushing, with the specimen undergoing lamina bending as the platen crushes the triggered length. At around 50mm of crushing, axial cracks start to appear along the side of the specimen. This causes the load bearing capacity to decrease until the specimen reaches compaction. Fibre fracture seen in the end result picture of Figure 4.7 (a) indicates that the specimen was efficiently propagating load energy towards the end of the crushing process.

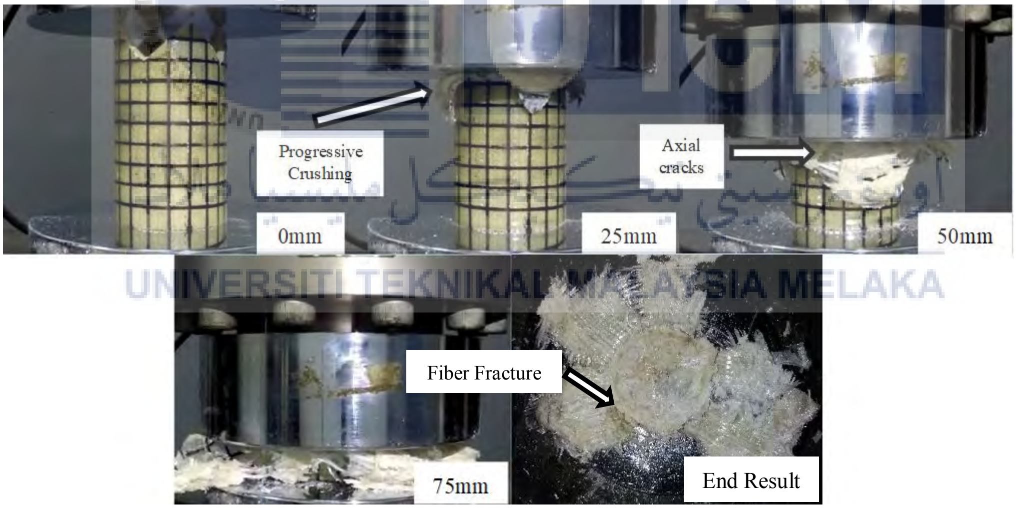

(a)

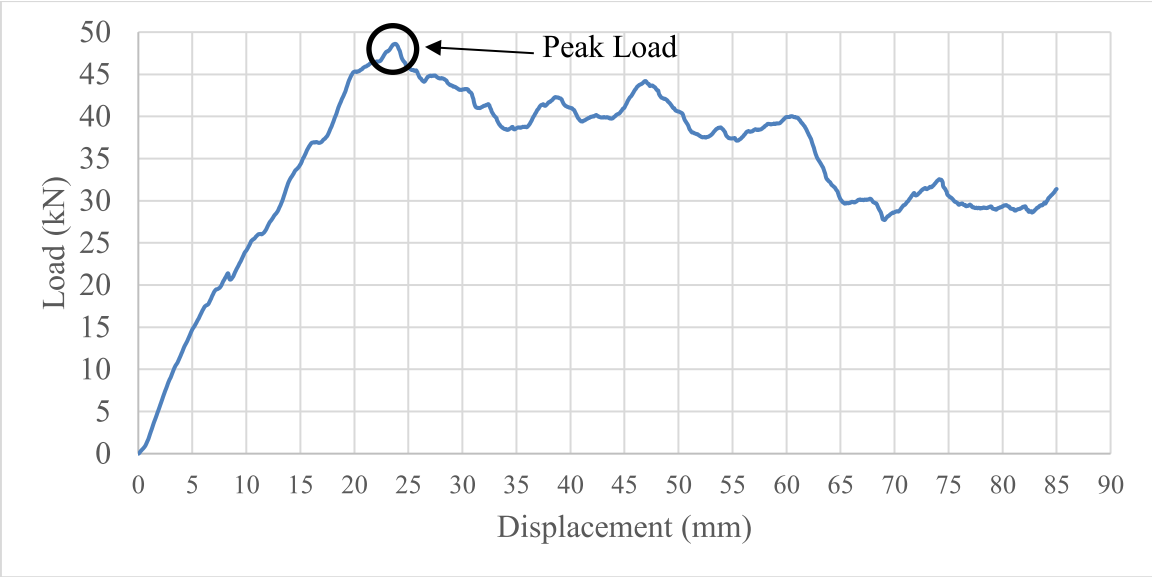

(b)

Figure 4.7: Quasi static compression test for tulip triggered GBG tube, (a) Photographs of specimen crushing at various stages and end result, (b) Load versus displacement during the crushing process.

4.3.3 BGB Lay-up Specimens

The graph in Figure 4.8 (a) show that the flat-ended BGB specimen reached the peak load of around 70 kN early in the crushing process, before 10mm of crushing extension, similar to other flat-ended specimens of different fibre sequence. Early axial cracks seen in the crushing sequence correlates with the critical drop in load in Fig 4.8 (b), as the specimen undergoes significant failure in terms of load bearing capacity. After the drop, the load vs extension graph fluctuates as the crushing progressed, which indicates progressive folding of the crushed specimen as seen in Figure 4.8 (a). A possible reason for this behaviour could be the presence of lamina bending and delamination in the specimen which could have encouraged the folding of delaminated layers, thus affecting the energy absorption capability of the specimen (Jiménez et al., 2000).

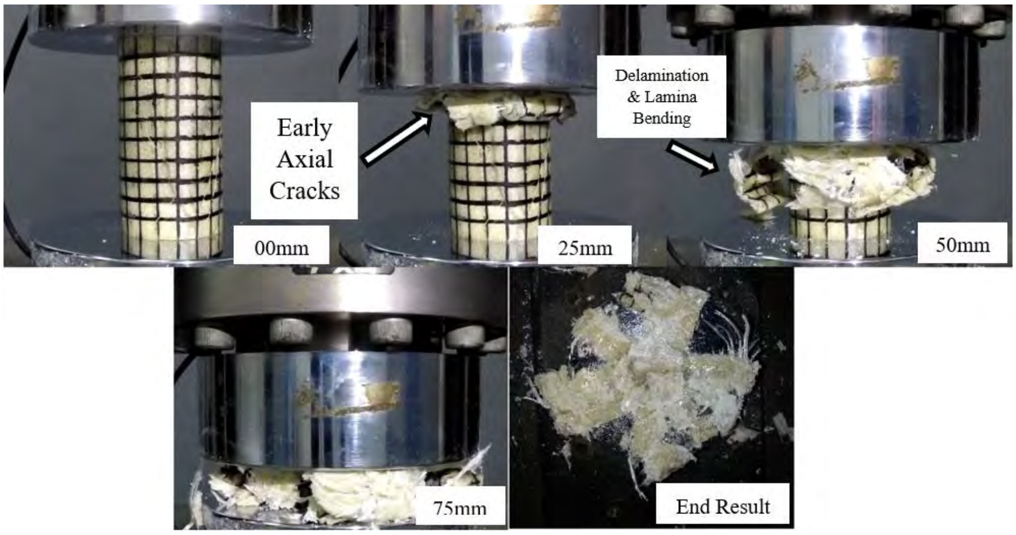

(a)

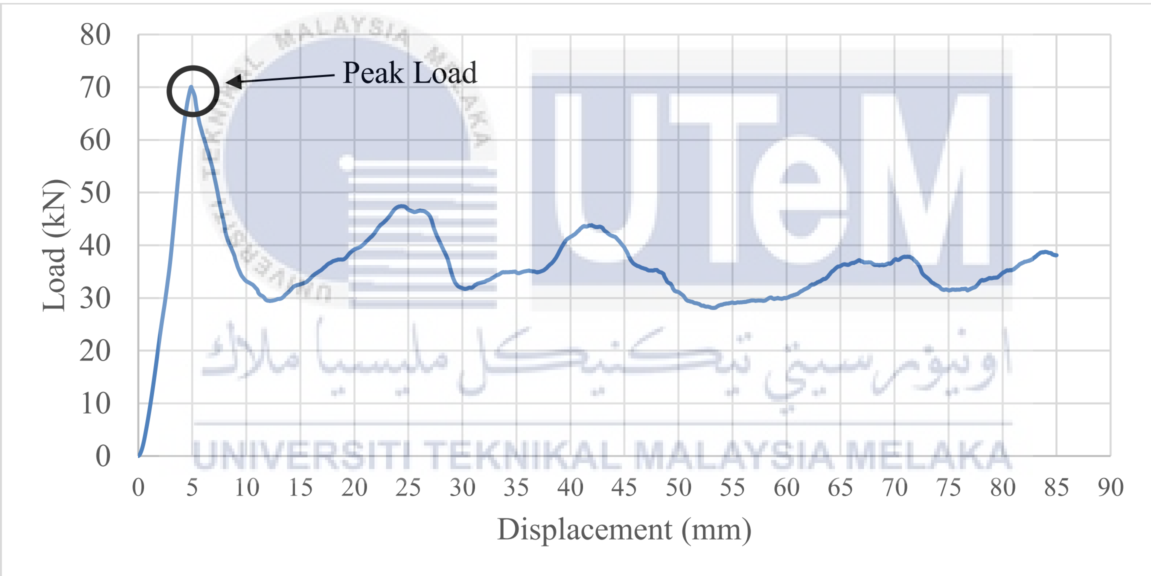

(b)

Figure 4.8: Quasi static compression test for flat-ended BGB tube, (a) Photographs of specimen crushing at various stages and end result, (b) Load versus displacement during the crushing process.

In Figure 4.9, the chamfer triggered BGB specimen exhibited a lower peak load value but achieved it similarly early as the flat-ended BGB sample. Moreover, the specimen also experienced a significant drop in load after achieving peak load. The appearance of early axial cracks could be a possible cause for this to occur. Despite that, the load increases between the crushing extension region of 10mm to 20mm and remains fairly stable until increasing in the compaction zone. A potential reason for this to happen is the development of lamina bending and slight delamination as the crushing progressed, indicating an efficient spreading of load force. This reasoning is further supported by the fibre fractures seen in the end result of Fig 4.9 (a).

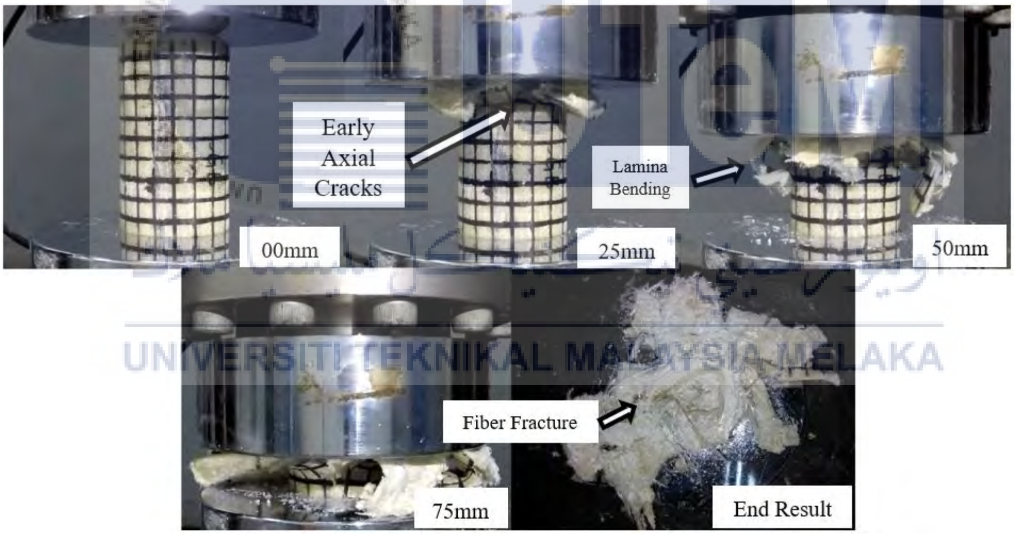

(a)

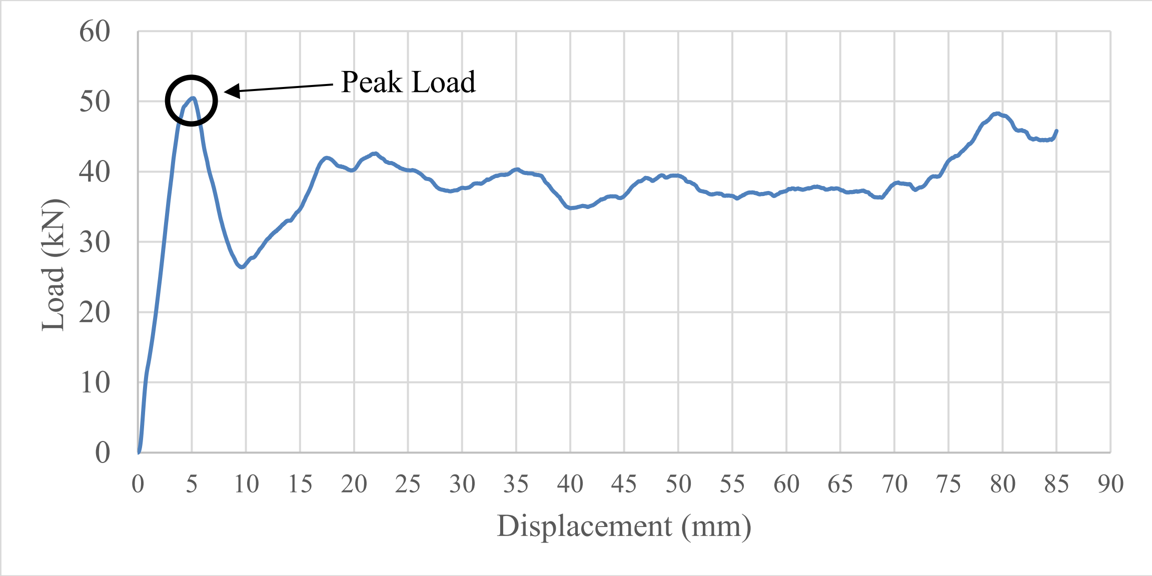

(b)

Figure 4.9: Quasi static compression test for chamfered BGB tube, (a) Photographs of specimen crushing at various stages and end result, (b) Load versus displacement during the crushing process.

Figure 4.10 that displays the crushing of the tulip triggered BGB sample provides further evidence of the tulip triggering mechanism lowering and delaying the peak load of the specimen. Unlike the other BGB specimen, the tulip triggered BGB sample does not undergo critical failure after achieving peak load. This is shown by the progressive crushing and lamina bending that occurred in Fig 4.10 (b), suggesting that crushing energy was distributed among the layers of fibre in the specimen. Further in the crushing process, load values fluctuate but ultimately decrease towards reaching the compaction zone. The spreading of axial cracks beginning from half of the crushing distance could have contributed to the load ultimately declining. In the end, fibre fractures show that the specimen was able to propagate the load energy in the final stages of crushing.

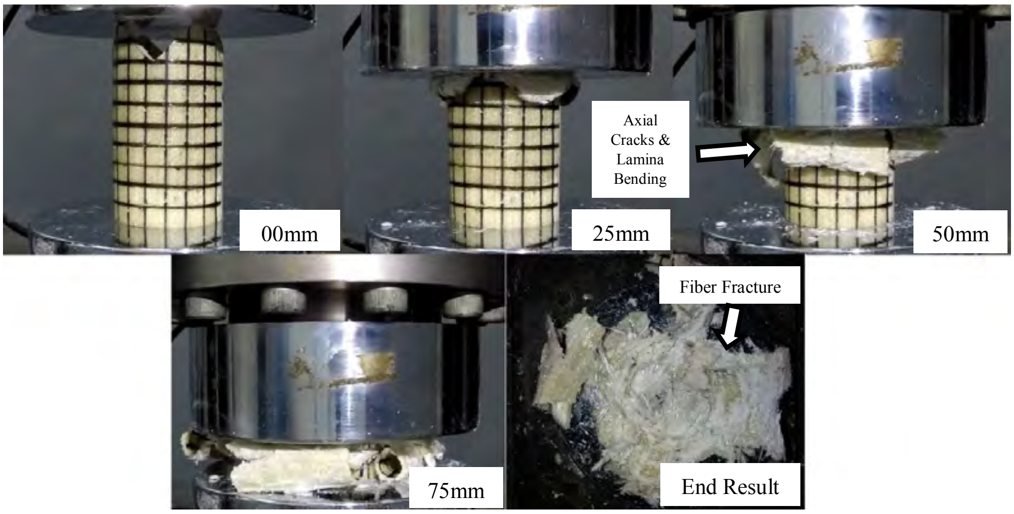

(a)

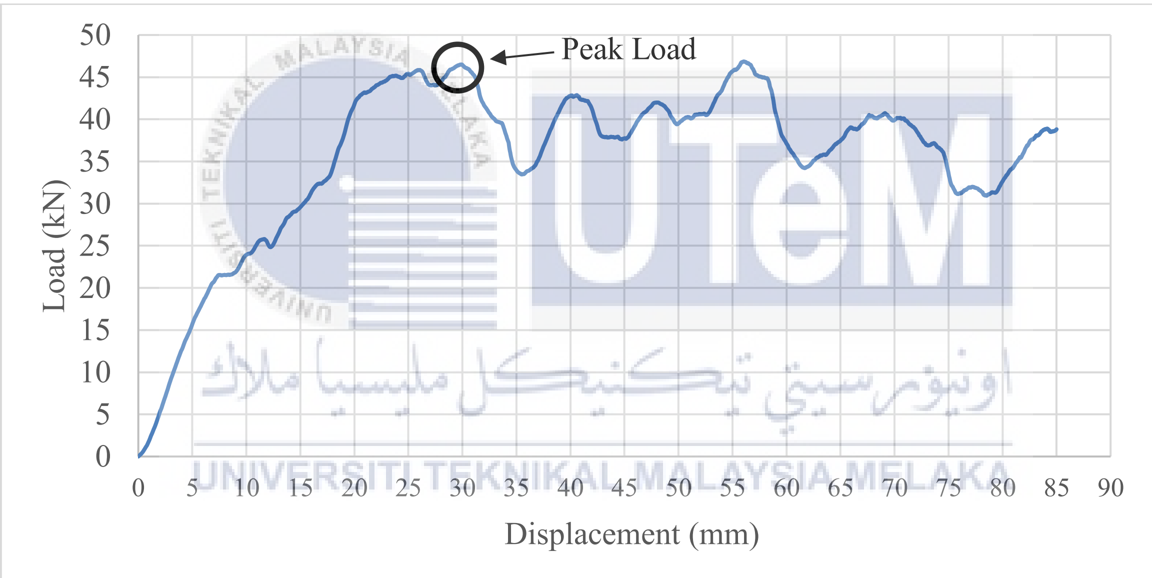

(b)

Figure 4.10: Quasi static compression test for tulip triggered BGB tube, (a) Photographs of specimen crushing at various stages and end result, (b) Load versus displacement during the crushing process.

4.3.4 BBB Lay-up Specimens

For the flat-ended BBB sample, Fig 4.11 demonstrates its energy absorption capabilities in a quasi-static crushing situation. After achieving an early peak load, the specimen suffered a catastrophic failure mode where there was an extreme drop in the load values. This is supplemented in Fig 4.11 (a), where a large axial split quickly formed during crushing. The split occurred in two places, resulting in the specimen almost being halved as the test progressed. This demonstrates the brittle nature of banana fibre composites when exposed to progressive loading. Further on, the specimen also underwent transverse failure when the walls of the specimen began to fold onto itself. Large pieces broke off from the specimen in Figure 4.11 (a) as a result of the transverse failures coupled with the axial splits.

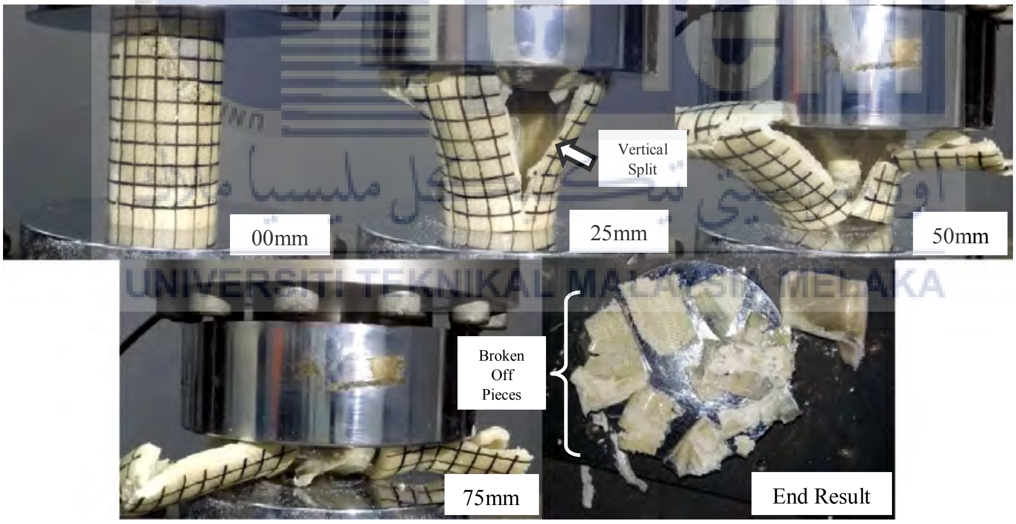

(a)

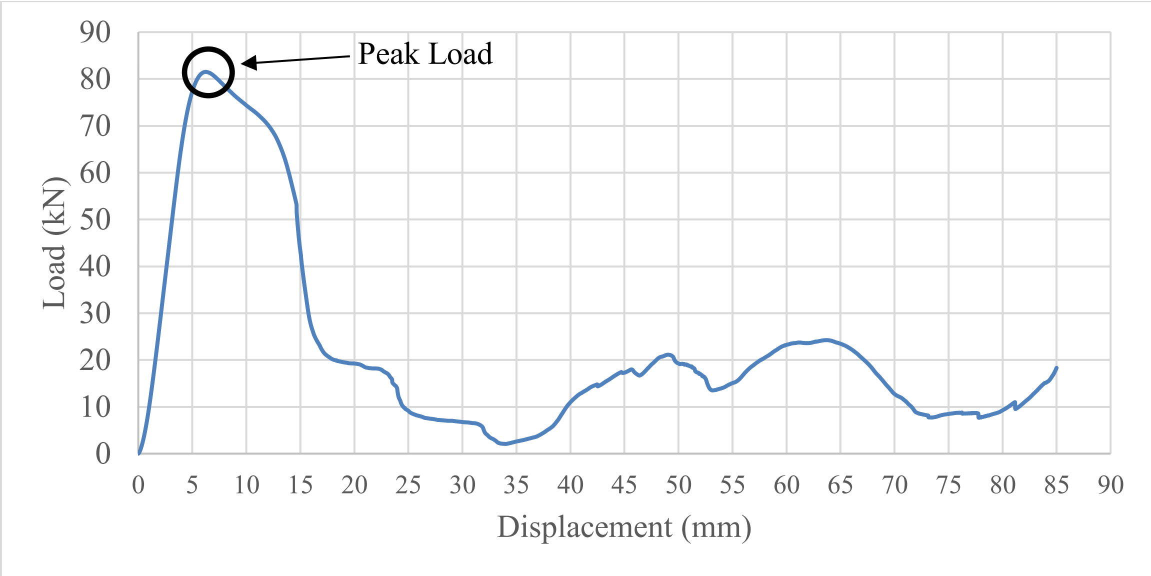

(b)

Figure 4.11: Quasi static compression test for flat-ended BBB tube, (a) Photographs of specimen crushing at various stages and end result, (b) Load versus displacement during the crushing process.

The quasi-static crushing behaviour of the chamfered BBB specimen is shown in Figure 4.12. The presence of a chamfer trigger mechanism allowed the specimen to decrease the peak load value by almost half compared to the flat-ended specimen of the same fibre sequence. Moreover, it only achieved the maximum force significantly later, within the 10mm to 20mm crushing extension region. The chamfer in this sample represents the most evident change in energy absorption characteristics compared to chamfer triggered specimens of other fibre sequences. However, the specimen formed axial cracks halfway throughout the crushing process, which resulted in the load values steadily declining. Transverse splits were formed when the specimen folded inwardly as the specimen reached the final stages of crushing, causing pieces to break off from the main body. This fold is also represented as a slight increase in load values from 50 to 70 mm of deformation.

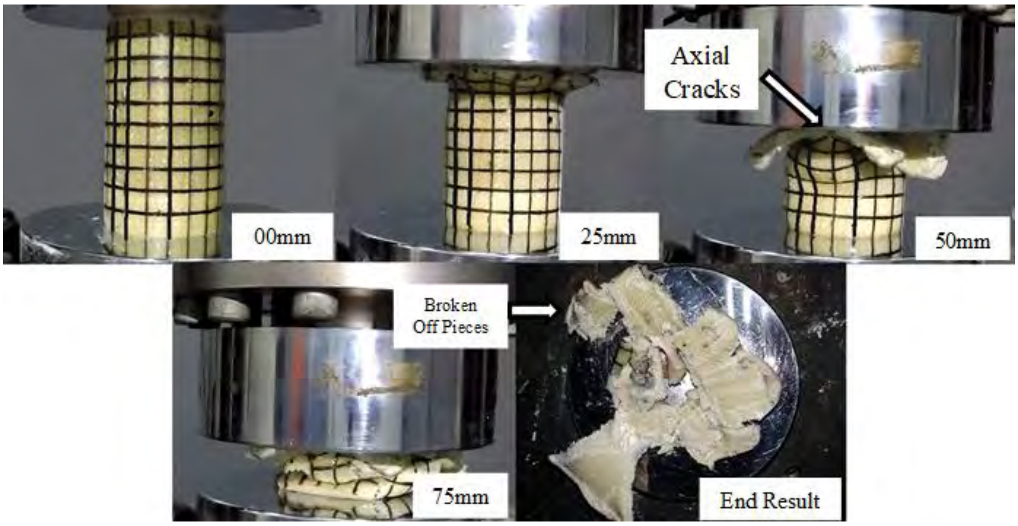

(a)

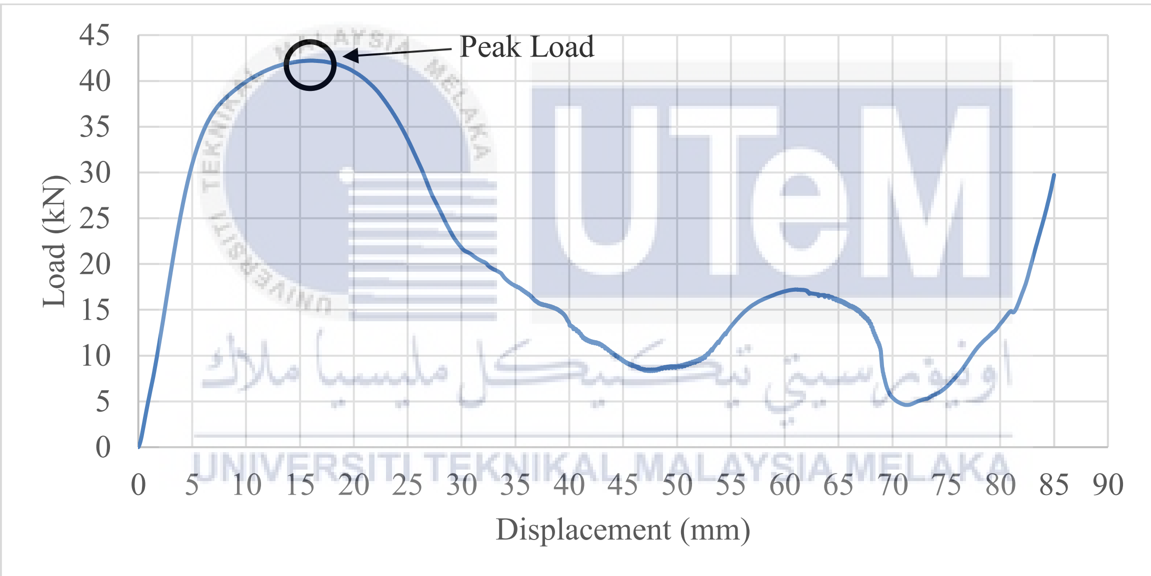

(b)

Figure 4.12: Quasi static compression test for chamfered BGB tube, (a) Photographs of specimen crushing at various stages and end result, (b) Load versus displacement during the crushing process.

The final configuration of specimens crushed is the tulip-triggered BBB specimens, as shown in Fig 4.13. Peak load of the sample was further reduced but occurred in the same region as the chamfered BBB specimen. The sample displayed progressive deformation as the triggered length of the specimen was crushed. A decrease in load values was observed around the 15mm to 30mm crushing extension region in Fig 4.13 (b) due to axial cracks starting to form at the corners of the tulip trigger. As crushing continued, the axial cracks began to bend and delaminate at the point of impact, causing a spike in load value halfway in the process. Appearance of fibre fractures and lamina bending in the end result of Figure 4.13 (a) proves that the specimen effectively spread the energy from crushing towards the end of the test.

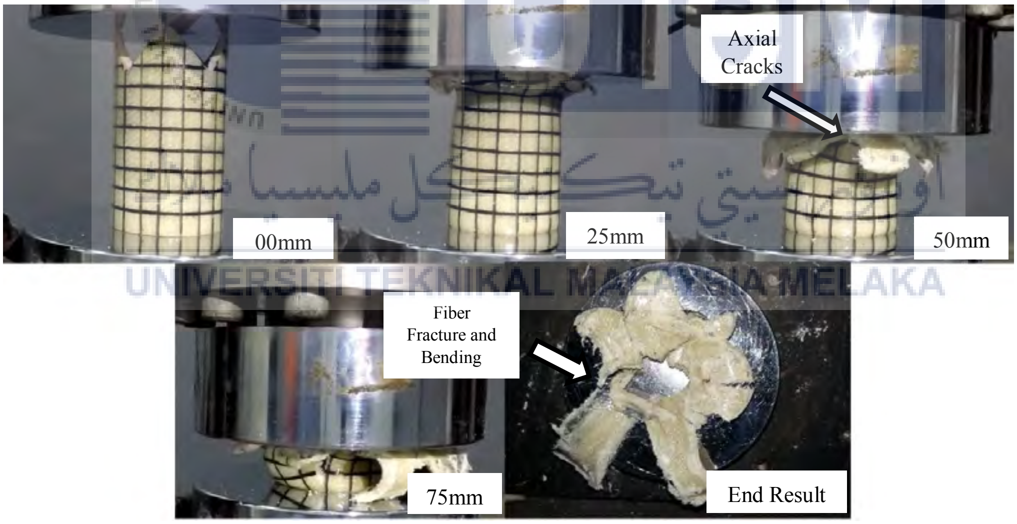

(a)

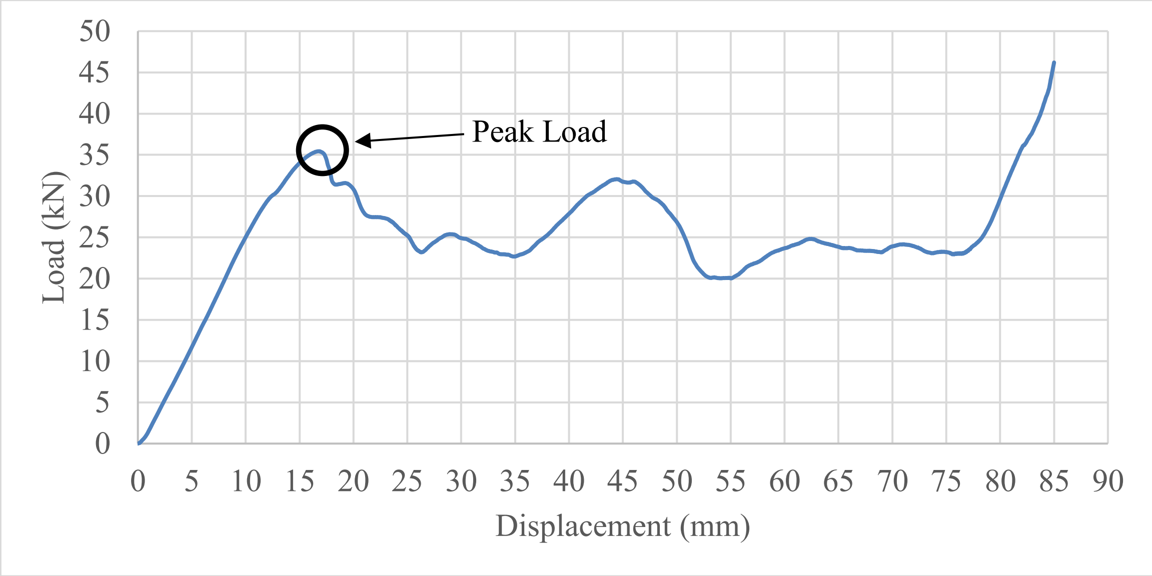

(b)

Figure 4.13: Quasi static compression test for tulip triggered BBB tube, (a) Photographs of specimen crushing at various stages and end result, (b) Load versus displacement during the crushing process.

4.4 Energy Absorption Characteristics

The average values for peak load, mean load, specific energy absorption and crush force efficiency are tabulated and presented in bar charts in the figures 4.14 to 4.19. The values are compared in terms of triggering mechanism within the same fibre lay-up sequence, and then a correlation between the energy absorption performance and fibre lay-up sequence. These comparisons will determine the most effective trigger mechanism and fibre lay-up sequence among the configurations tested. "NT" in the bar chart refers to flat-ended, while "CT" and "TT" specifies specimens of chamfer trigger and tulip trigger respectively. The level of significance between parameters to determine energy absorption capability in decreasing order goes as specific energy absorption, mean load, peak load and crush force efficiency. Values for figures 4.14 to 4.19 are tabulated in Appendix B.

The average peak load (Figure 4.14) achieved by specimens reveal that the flat-ended specimen achieved the highest value in all fibre lay-up sequences, as the flat-ended BGB sample reaching a peak load of 61.9704 kN. This finding is in line with the research done by Pitarresi et al. and Siromani et al. (2014), where the specimens with triggering mechanism reported lower values of peak load when reviewed against flat-ended specimens. Moreover, the tulip trigger was more effective in lowering the peak load in the GGG, BGB and BBB samples compared to the chamfer triggered samples, with the tulip GGG sample reaching the lowest value of 18.3338 kN. A lower value of peak load indicates that the specimen was able to remain in the plastic deformation region longer before failure. Chamfer and tulip triggers are able to delay (Figure 4.15) and lower the peak load of the specimen. A study conducted by Chiu et al. in 2015 that obtained a similar trend of results concluded that peaks of tulip and chamfer triggers act as points for damage initiation. As the peaks are easily deformed, these initiation points allow the damage to be propagated evenly throughout the whole specimen. Tulip triggers are proven to be more effective due to the crushing beginning at the peaks, then gradually increasing as the tulip width increases.

In terms of fibre lay-up sequence, the GGG sequence presented a greater variance in peak load for the flat-ended specimen compared to the other GGG specimens. Both the hybrid GBG and BGB specimens display less variations in terms of peak load values between specimens of different triggers. Specimens with banana fibre in the sequence achieved a higher general peak load value than the GGG specimens. A study by Zin et. al. in 2018 determined that banana fibre samples have high flexural strength compared to samples of glass fibre. This suggests that the GBG, BGB and BBB fibre configurations allow the specimen to remain longer in the plastic deformation region during the quasi-static crushing test, therefore achieving higher peak load values.

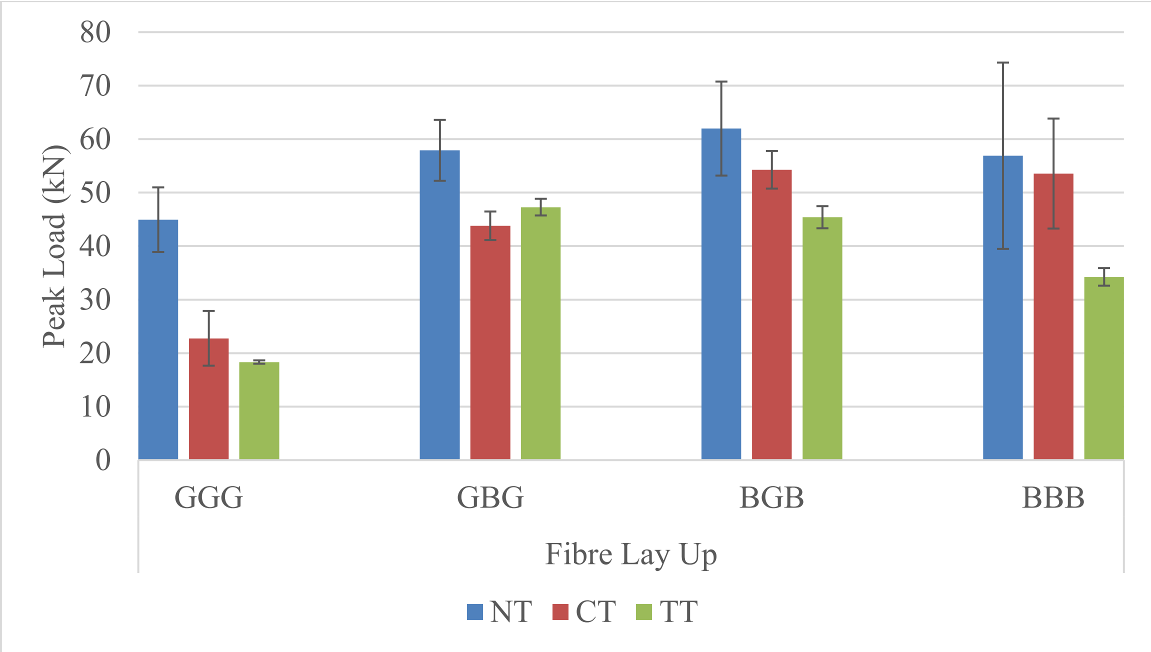

Figure 4.14: Peak load for varying trigger and lay-up

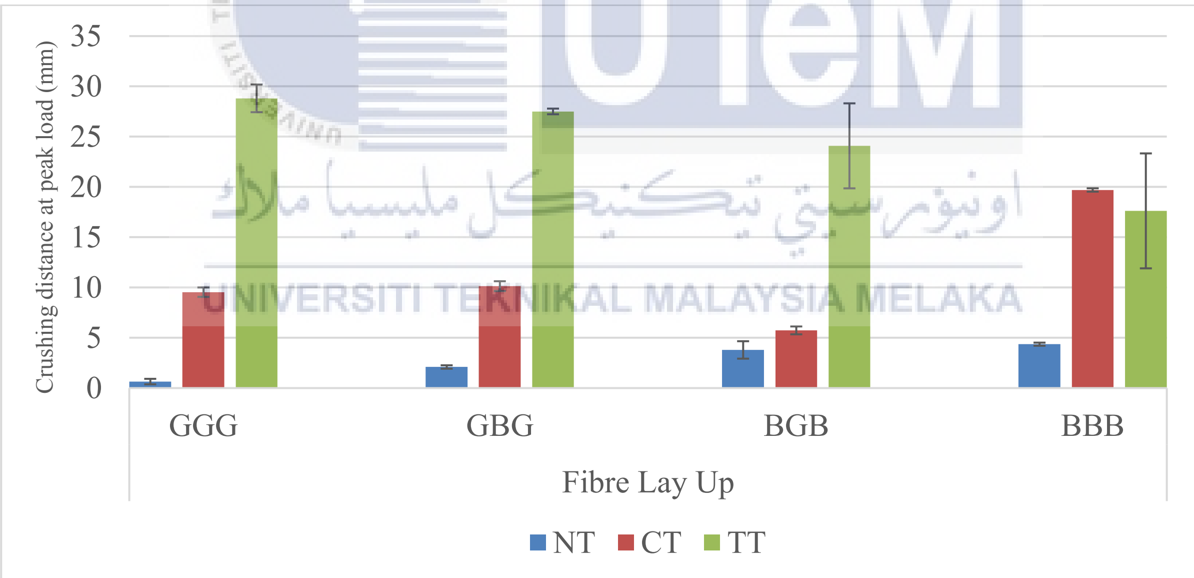

Figure 4.15: Crushing distance of specimen during peak load

Figure 4.16 compares the mean load values obtained by the specimens through the quasi-static crushing test. Tulip triggered specimens from all fibre sequences exhibited a higher mean load when compared with the chamfer-triggered and flat-ended specimens. Mean load represents area under the graph starting from peak load to the start of compaction. This provides an insight into the post-failure energy absorbing capabilities of the specimen. Chamfered specimens also display higher average mean load values than flat-ended samples. This was due to the flat-ended specimens undergoing catastrophic failure after achieving peak load. Flat-ended specimens are not able to sustain the load throughout the crushing process because of damages such as axial cracks and splits. These damages form after peak load, and spreads as the crushing progresses. Tulip triggers excel in post-failure energy absorption due to the aforementioned load initiation peaks encouraging delamination and lamina bending as the crushing process continues past the triggered length (Chiu et al., 2015).

Mean load values in Figure 4.16 also characterise energy absorbing characteristics of composite specimens with different fibre lay-up sequences. From the figure, it is apparent that that the specimens of hybrid GBG and BGB configurations exhibit increased values of mean load compared to the GGG and BBB sequence specimens. Possible reasons for this occurrence include short crushing distance in the post-crushing zone (Figure 4.17), or higher total load accumulated in the same zone. The shorter crushing distance is the result of flexural strength of banana fibre which also increased peak load in Fig 4.16. GBG and BGB specimens also reported higher total load accumulated in the post-crushing zone, due to both inherent properties of glass and banana fibre affecting the reaction of specimens to crushing load. (Sathish et al., 2015)

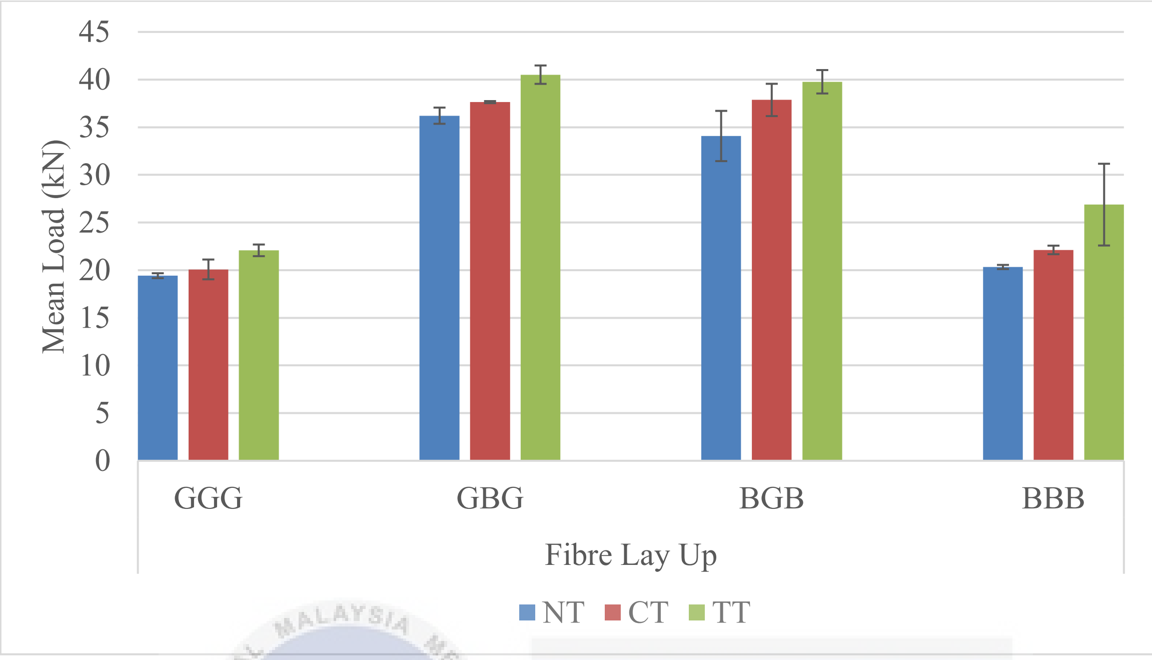

Figure 4.16: Mean load for varying trigger and layup

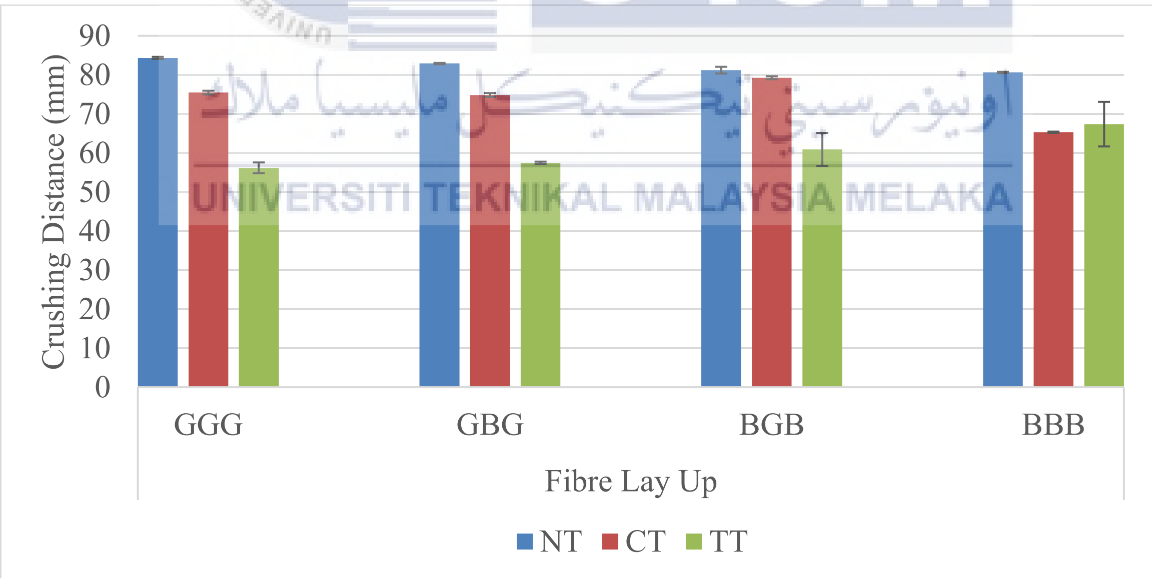

Figure 4.17: Length of crushing distance in post-crushing zone for varying trigger and lay-up

Figure 4.18 shows the specific energy absorption (SEA) values of the fibre composite specimens. SEA provides an accurate representation of how trigger mechanisms and fibre lay-up sequence affect load bearing capacity of specimens in applications where weight is considered, such as in the automotive and aviation industries. From the figure, it is apparent that tulip triggered specimens performed better as SEA values achieved are higher, with BGB specimen achieving 28.8869 kJ/kg, than the chamfered and flat-ended specimens of BBB sequence that achieved 11.3986 kJ/kg and 13.3556 kJ/kg respectively. SEA values of the GBG tulip specimen was higher by 30.65% compared to the flat-ended GBG specimen. This proves that specimens with tulip trigger mechanisms were able to sustain load efficiently even after losing weight after trigger fabrication. Moreover, the higher average mean load achieved by tulip-triggered specimens also correlates to the higher SEA values. These results agree with the findings of other studies, in which it was found that tulip triggers cause V cracks to form in the wall of the specimen (Palanivelu et al., 2011; Huang & Wang 2010). Huang & Wang (2010) found that these cracks aid the specimen in sustaining load by encouraging delamination in the post-crushing region.

Fibre lay-up sequence also affects the SEA values obtained by composite specimens, where weight of the specimen is a factor. SEA values of specimens follow the trend of values in Figure 4.18, where values of SEA obtained by the hybrid composites are higher than those of single fibre type configuration. This result is supplemented by other literature studies, most notably a research by Attia et al. in 2017, where hybrid composites of symmetrical glass and jute fibre lay-up sequences displayed superior SEA values compared to single fibre or asymmetrical sequence composite tubes. Attia et. al. (2017) credit this phenomenon to the natural fibres having a higher modulus of elasticity, therefore increasing bending stiffness which increases SEA as a result.

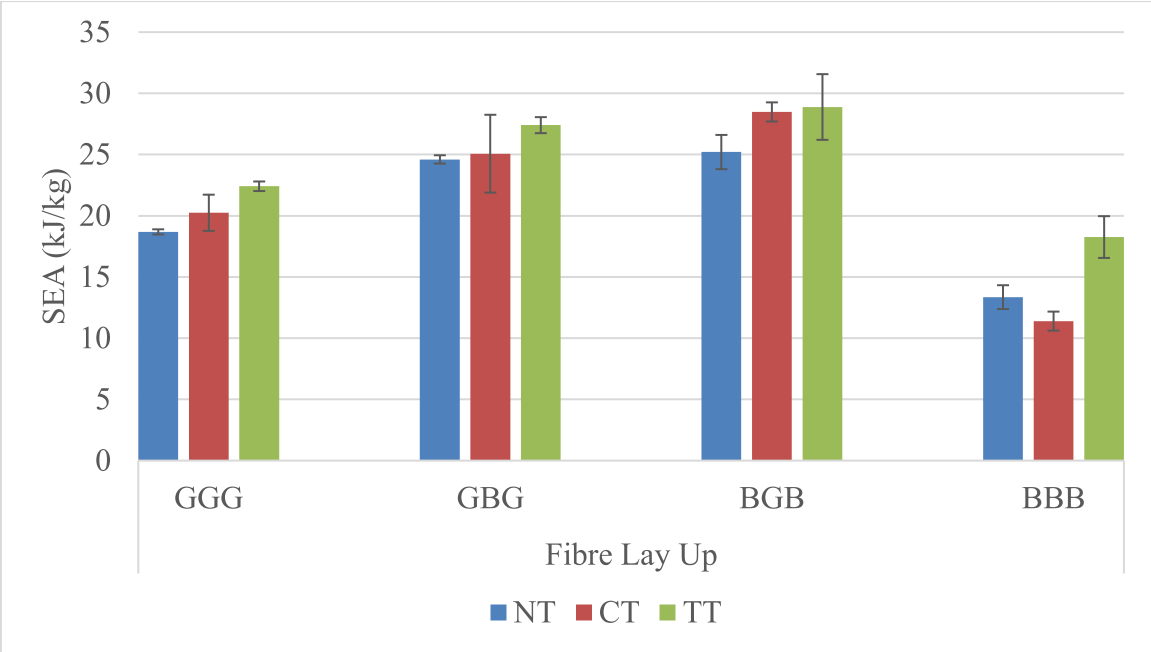

Figure 4.18: Specific energy absorption values

Figure 4.19 represent the crush force efficiency (CFE) valuation from the quasi-static crushing test. CFE is defined as the ratio of mean load to the peak load obtained by the specimen. The value of CFE can be elevated if the value of mean load is closer to the peak load achieved. A value close to or above unity is sought after, which suggests stable deformation during the crushing test (Sivagurunathan et al., 2018). In terms of triggering mechanism, Figure 4.19 shows that tulip-triggered specimens attained the higher average CFE value in the GGG, BGB and BBB specimens, with the tulip-triggered GGG specimen achieving the highest average CFE of 1.2054. Interestingly, the chamfered specimen of GBG fibre sequence achieved a higher CFE compared to the rest of the GBG specimens. This uncommon finding could have occurred due to variations in fibre properties or differences in wall thickness of specimens. Flat-ended specimens demonstrate a general trend of obtaining the lowest CFE values in all fibre sequence configurations. This is likely due to the higher peak load achieved by the flat-ended samples, thus causing the CFE values to plummet.

Interestingly, the findings presented in Figure 4.19 do not replicate the trend in the results of other energy absorption characteristics like peak load, mean load and SEA. The chart shows that the GGG specimen achieved a generally higher value of crush force efficiency (CFE) among the other specimens with different fibre lay-up sequence. Moreover, all three configurations of GGG samples experienced progressive crushing after achieving peak load, which led to a high total load in post-crushing zone. However, the value of CFE does not accurately represent energy absorbing capability and is low priority among the other parameters tested.

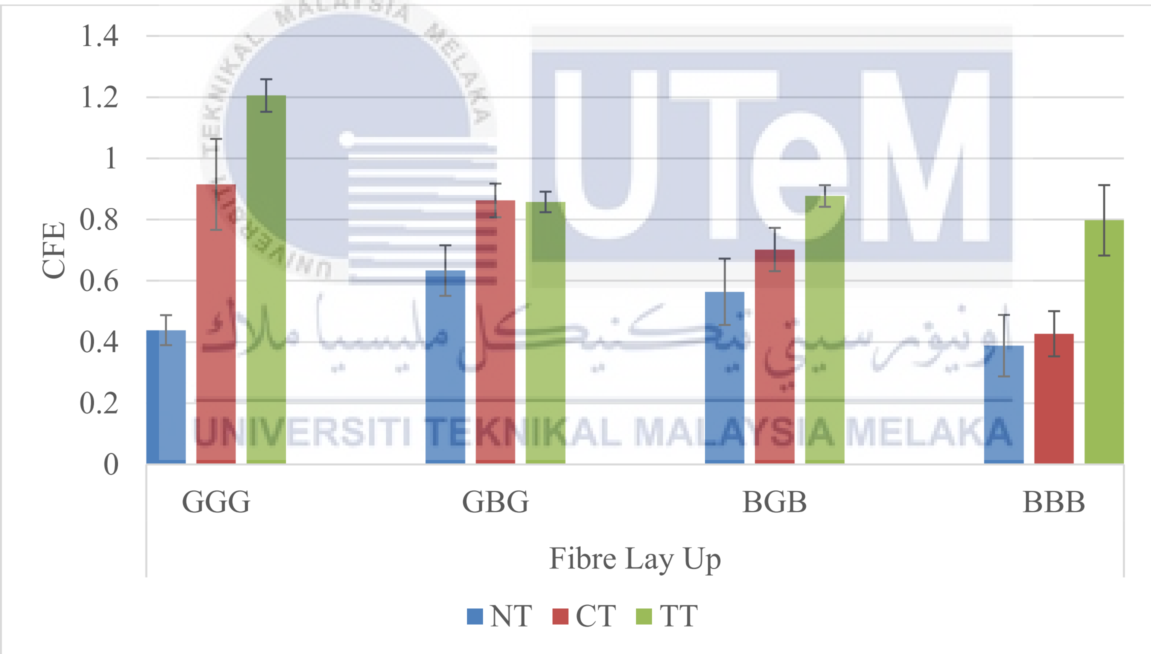

Figure 4.19: Crush force efficiency values

CHAPTER 5

CONCLUSION

5.1 Summary

Past literature on fibre composites show that triggering mechanisms, differing lay-up and other parameters involved in the fabrication process of composites significantly affect its energy absorbing capabilities.

In this study, the quasi-static crushing was carried on composites tubes with different fibre lay-up sequence and triggering mechanism. Based on the data obtained from the quasi-static crushing test, it can be summarised that tulip-triggered specimens exhibited better energy absorption characteristics during the crushing process, such as delamination, lamina bending and fibre fracture. Moreover, mean load, SEA and CFE values obtained show that tulip-triggered specimens significantly improve the energy absorption of fibre composite specimens. The average SEA for tulip specimen of BGB fibre sequence is higher by 8.51% compared to the chamfered specimens, and 10.22% higher compared to the flat-ended specimens of the same fibre lay-up sequence.

In terms of fibre lay-up sequence, the hybrid sequences GBG and BGB demonstrate superior energy absorption capability compared to single fibre sequence composites such as GGG and BBB. The crushing test shows that the hybridisation of fibre in composites does improve the crashworthiness characteristics when tested in a quasi-static crushing test.

5.2 Recommendations

For further research into fibre reinforced composites, many parameters can be altered and many variables can be tested. These variables will provide insight on the effects they have on the energy absorption capability of the composite specimen tested. The diameter to thickness (*d/t*) ratio of the fabricated specimens can be altered to determine the effects of cross-sectional area and geometry on composite crashworthiness. Moreover, tulip-triggered and chamfer-triggered specimens can be analysed and compared with the performance of crown-triggered composites. The crown triggering mechanism is a hybrid of both chamfer and tulip triggers, and its effects are currently being researched.

The orientation angle of fibres in the lay-up process can also be changed when fabricating composites. Fibres can be stacked in sequences of varying angles to determine the crush response of composites to the angle of fibre. Furthermore, composites with the same configuration, geometry and lay-up can be fabricated using varying techniques. Composite specimens can be made by vacuum assisted resin transfer moulding, wet hand lay-up and bladder assisted moulding and then tested to determine the effectiveness of the technique in fabricating crashworthy composites.

REFERENCES

Abdullah, N., & Ismail, A. E. (2017). Axial quasi-static crushing behaviour of cylindrical woven kenaf fiber reinforced composites. In *IOP Conference Series: Materials Science and Engineering* (Vol. 165).

Alia, R. A., Cantwell, W. J., Langdon, G. S., Yuen, S. C. K., & Nurick, G. N. (2014). The energy-absorbing characteristics of composite tube-reinforced foam structures. *Composites Part B: Engineering*, *61*, 127–135.

Anderson, J. P., & Altan, M. C. (2016). Reduction of microvoids in composite laminates fabricated by bladder assisted composite manufacturing (BACM). *Polymer Composites*, *37*(2), 561–572.

Ataollahi, S., Taher, S. T., Eshkoor, R. A., Ariffin, A. K., & Azhari, C. H. (2012). Energy absorption and failure response of silk/epoxy composite square tubes: Experimental. *Composites Part B: Engineering*, *43*(2), 542–548.

Attia, M. A., Abd El-Baky, M. A., Hassan, M. A., Sebaey, T. A., & Mahdi, E. (2017). Crashworthiness characteristics of carbon-jute-glass reinforced epoxy composite circular tubes. *Polymer Composites*, 1–17.

Chiu, L. N. S., Falzon, B. G., Ruan, D., Xu, S., Thomson, R. S., Chen, B., & Yan, W. (2015). Crush responses of composite cylinder under quasi-static and dynamic loading. *Composite Structures*, *131*, 90–98.

Courteau, M. A. (2011). Investigating the crashworthiness characteristics of carbon fiberepoxy tubes. *University of Utah*, (December).

Eshkoor, R. A., Oshkovr, S. A., Sulong, A. B., Zulkifli, R., Ariffin, A. K., & Azhari, C. H. (2013). Effect of trigger configuration on the crashworthiness characteristics of natural silk epoxy composite tubes. *Composites Part B: Engineering*, *55*(1), 5–10.

Eshkoor, R. A., Ude, A. U., Sulong, A. B., Zulkifli, R., Ariffin, A. K., & Azhari, C. H. (2015). Energy absorption and load carrying capability of woven natural silk epoxy - Triggered composite tubes. *Composites Part B: Engineering*, *77*. 10-18

Gonzalez-Canche, N. G., Flores-Johnson, E. A., & Carrillo, J. G. (2017). Mechanical characterization of fiber metal laminate based on aramid fiber reinforced polypropylene. *Composite Structures*, *172*, 259-266.

Gopal, Y., & Ramnath, V. (2016). Investigation Of Flexural And Water Absorption Behaviour Of Epoxy Hybrid Composites, (February 2017).

Hitchen, S. A., & Kemp, R. M. J. (1995). The effect of stacking sequence on impact damage in a carbon fibre/epoxy composite. *Composites*, *26*(3), 207–214.

Hosseini, S. M., & Shariati, M. (2018). Experimental analysis of energy absorption capability of thin-walled composite cylindrical shells by quasi-static axial crushing test. *Thin-Walled Structures*, *125*, 259–268.

Hu, D., Zhang, C., Ma, X., & Song, B. (2016). Effect of fiber orientation on energy absorption characteristics of glass cloth/epoxy composite tubes under axial quasi-static and impact crushing condition. *Composites Part A: Applied Science and Manufacturing*, *90*, 489–501.

Huang, J. C., & Wang, X. W. (2010). Effect of the SMA trigger on the energy absorption characteristics of CFRP circular tubes. *Journal of Composite Materials*, *44*(5), 639–651.

Huang, J., & Wang, X. (2010). On a new crush trigger for energy absorption of composite tubes. *International Journal of Crashworthiness*. *15(6)*, 625-634.

Jackson, A., Dutton, S., Gunnion, A. J., & Kelly, D. (2011). Investigation into laminate design of open carbon-fibre/epoxy sections by quasi-static and dynamic crushing. *Composite Structures*, *93*(10), 2646–2654.

Jiménez, M. A., Miravete, A., Larrodé, E., & Revuelta, D. (2000). Effect of trigger geometry on energy absorption in composite profiles. *Composite Structures*, *48(1-3)*, 107-111.

Kaneko, S., Mele, P., Endo, T., Tsuchiya, T., Tanaka, K., Yoshimura, M., & Hui, D. (2017). Energy Absorption Capability of Hybrid Fibers Reinforced Composite Tubes. *Carbon-Related Materials in Recognition of Nobel Lectures by Prof. Akira Suzuki in ICCE*, 145-173.

Kim, J. S., Yoon, H. J., & Shin, K. B. (2011). A study on crushing behaviors of composite circular tubes with different reinforcing fibers. *International Journal of Impact Engineering*, *38*(4), 198–207.

Kim, S. Y., Shim, C. S., Sturtevant, C., Kim, D. D. W., & Song, H. C. (2014). Mechanical properties and production quality of hand-layup and vacuum infusion processed hybrid composite materials for GFRP marine structures. *International Journal of Naval Architecture and Ocean Engineering*, *6(3)*, 723-736.

Luo, H., Yan, Y., Meng, X., & Jin, C. (2016). Progressive failure analysis and energy-absorbing experiment of composite tubes under axial dynamic impact. *Composites Part B: Engineering*, *87*, 1–11.

Meredith, J., Ebsworth, R., Coles, S. R., Wood, B. M., & Kirwan, K. (2012). Natural fibre composite energy absorption structures. *Composites Science and Technology*, *72*(2), 211–217.

Padam, B. S., Tin, H. S., Chye, F. Y., & Abdullah, M. I. (2014). Banana by-products: an under-utilized renewable food biomass with great potential. *Journal of Food Science and Technology*, *51(12)*, 3527-3545.

Palanivelu, S., Paepegem, W. Van, Degrieck, J., Vantomme, J., Kakogiannis, D., Ackeren, J. Van, Wastiels, J. (2011). Crushing and energy absorption performance of different geometrical shapes of small-scale glass/polyester composite tubes under quasi-static loading conditions. *Composite Structures*, *93*(2), 992–1007.

Pickett, L., & Dayal, V. (2012). Effect of tube geometry and ply-angle on energy absorption of a circular glass/epoxy crush tube - A numerical study. *Composites Part B: Engineering*, *43*(8), 2960–2967.

Pitarresi, G., Carruthers, J. J., Robinson, A. M., Torre, G., Kenny, J. M., Ingleton, S., Found, M. S. (2007). A comparative evaluation of crashworthy composite sandwich structures. *Composite Structures*, *8(1)*, 34-44.

Ramakrishna, S., & Hull, D. (1993). Energy absorption capability of epoxy composite tubes with knitted carbon fibre fabric reinforcement. *Composites Science and Technology*, *49*(4), 349–356.

Sanjay, M. R., & Yogesha, B. (2016). Studies on Mechanical Properties of Jute / E-Glass Fiber Reinforced Epoxy Hybrid Composites. *Journal of Minerals and Materials Characterization and Engineering*, *4.0*(January), 15–25.

Sathish, P., Kesavan, R., Ramnath, B. V., & Vishal, C. (2015). Effect of Fiber Orientation and Stacking Sequence on Mechanical and Thermal Characteristics of Banana-Kenaf Hybrid Epoxy Composite. *Silicon*, *9(4)*, 577-585.

Sigalas, I., Kumosa, M., & Hull, D. (1991). Trigger mechanisms in energy-absorbing glass cloth/epoxy tubes. *Composites Science and Technology*, *40*(3), 265–287.

Siromani, D., Henderson, G., Mikita, D., Mirarchi, K., Park, R., Smolko, J., Tan, T. M. (2014). An experimental study on the effect of failure trigger mechanisms on the energy absorption capability of CFRP tubes under axial compression. *Composites Part A: Applied Science and Manufacturing*, *64*, 25–35.

Sivagurunathan, R., Lau Tze Way, S., Sivagurunathan, L., & Yaakob, M. Y. (2018). The Effects of Triggering Mechanisms on the Energy Absorption Capability of Circular Jute/Epoxy Composite Tubes under Quasi-Static Axial Loading. *Applied Composite Materials*, *25(6)*, 1401-1417.

Stamenovic S; Zrilic, M; Milovic, Lj; Pavlovic-krstic, J;, M. P. (2011). Specific energy absorption capacity of glass-polyester composite tubes under static compressive loading. *Metalurgija Volume 50 Issue 3 (Pp 197-200)*.

Wang, Y., Feng, J., Wu, J., & Hu, D. (2016). Effects of fiber orientation and wall thickness on energy absorption characteristics of carbon-reinforced composite tubes under different loading conditions. *Composite Structures*, *153*, 356–368.

Zheng, N., Huang, Y., Liu, H. Y., Gao, J., & Mai, Y. W. (2017). Improvement of interlaminar fracture toughness in carbon fiber/epoxy composites with carbon nanotubes/polysulfone interleaves. *Composites Science and Technology*, *140*, 8–15.

Zin, M. H., Abdan, K., & Norizan, M. N. (2019). The effect of different fiber loading on flexural and thermal properties of banana/pineapple leaf (PALF)/glass hybrid composite. *Structural Health Monitoring of Biocomposites, Fibre-Reinforced Composites and Hybrid Composites*, 1-17.

APPENDIX

APPENDIX A

Table A1: Physical properties of GGG specimens

Specimen	Trigger Mechanism	Mass (kg)	Length (mm)	Outer Diameter, D_o (mm)	Thickness (mm)			
					1	2	3	AVG
GGG - NT (1)	No	0.066	100.00	5.730	2.55	2.60	2.25	2.47
GGG - NT (2)	No	0.057			2.20	2.75	2.52	2.49
GGG - NT (3)	No	0.067			2.10	2.20	2.45	2.25
GGG - CT (1)	45° Chamfer	0.052			2.00	2.70	2.55	2.41
GGG - CT (2)	45° Chamfer	0.062			2.30	2.00	2.40	2.23
GGG - CT (3)	45° Chamfer	0.054			2.30	2.50	2.35	2.38
GGG - TT (1)	Tulip	0.045			2.20	1.70	1.70	1.87
GGG - TT (2)	Tulip	0.045			1.90	2.10	1.90	1.98
GGG - TT (3)	Tulip	0.046			1.70	2.10	1.70	1.83

Table A2: Physical properties of GBG specimens

Specimen	Trigger Mechanism	Mass (kg)	Length (mm)	Outer Diameter, D_o (mm)	Thickness (mm)			
					1	2	3	AVG
GBG - NT (1)	No	0.101	100.00	5.730	4.60	5.00	5.50	5.03
GBG - NT (1)	No	0.104			4.70	5.05	4.40	4.72
GBG - NT (1)	No	0.101			4.80	5.50	4.40	4.90
GBG - CT (1)	45° Chamfer	0.101			4.20	4.55	5.60	4.78
GBG - CT (2)	45° Chamfer	0.105			5.50	4.25	4.70	4.82
GBG - CT (3)	45° Chamfer	0.096			5.55	4.60	5.00	5.05
GBG - TT (1)	Tulip	0.091			5.60	4.90	4.95	5.15
GBG - TT (2)	Tulip	0.085			5.25	4.05	5.20	4.83
GBG - TT (3)	Tulip	0.092			4.30	5.90	5.50	5.23

Table A3: Physical properties of BGB specimens

Specimen	Trigger Mechanism	Mass (kg)	Length (mm)	Outer Diameter, Do (mm)	Thickness (mm)			
					1	2	3	AVG
BGB - NT (1)	No	0.114	100.00	5.730	6.70	5.95	5.40	6.02
BGB - NT (2)	No	0.108			6.00	5.25	6.50	5.92
BGB - NT (3)	No	0.107			6.00	5.10	5.45	5.52
BGB - CT (1)	45° Chamfer	0.108			5.90	5.40	5.50	5.60
BGB - CT (2)	45° Chamfer	0.102			5.05	5.20	5.40	5.22
BGB - CT (3)	45° Chamfer	0.106			5.15	5.50	5.55	5.40
BGB - TT (1)	Tulip	0.095			5.95	4.75	5.80	5.50
BGB - TT (2)	Tulip	0.094			6.05	5.05	5.30	5.47
BGB - TT (3)	Tulip	0.093			5.50	4.70	5.40	5.20

Table A4: Physical properties of BBB specimens

Specimen	Trigger Mechanism	Mass (kg)	Length (mm)	Outer Diameter, Do (mm)	Thickness (mm)			
					1	2	3	AVG
BBB - NT (1)	No	0.121	100.00	5.730	6.00	5.55	6.50	6.02
BBB - NT (2)	No	0.115			5.85	5.90	5.70	5.82
BBB - NT (3)	No	0.134			6.65	6.60	6.05	6.43
BBB - CT (1)	45° Chamfer	0.135			6.25	7.15	7.50	6.97
BBB - CT (2)	45° Chamfer	0.132			7.50	6.70	7.80	7.33
BBB - CT (3)	45° Chamfer	0.115			5.75	6.10	6.80	6.22
BBB - TT (1)	Tulip	0.099			6.20	6.05	6.30	6.18
BBB - TT (2)	Tulip	0.094			5.80	6.25	6.30	6.12
BBB - TT (3)	Tulip	0.101			6.20	5.20	6.15	5.85

APPENDIX B

Table B1: Peak load values

Fibre Sequence	Triggering Mechanism	Peak Load (kN)				
		Specimen			Average	Std. Dev.
		1	2	3		
GGG	No	41.6140	53.4274	39.7916	44.9443	6.0444
	45 Chamfer	17.7001	20.8160	29.7802	22.7655	5.1207
	Tulip	18.1592	18.0604	18.7819	18.3338	0.3194
GBG	No	62.5520	49.8808	61.2769	57.9033	5.6965
	45 Chamfer	45.2973	46.0619	40.0572	43.8055	2.6687
	Tulip	45.1056	48.1528	48.6121	47.2902	1.5560
BGB	No	70.0691	49.7572	66.0848	61.9704	8.7879
	45 Chamfer	50.4515	58.9421	53.4205	54.2713	3.5181
	Tulip	46.5003	47.2080	42.5175	45.4086	2.0646
BBB	No	44.5168	44.6465	81.5232	56.8955	17.4145
	45 Chamfer	51.3733	67.1025	42.2115	53.5625	10.2789
	Tulip	33.5319	35.4438	31.9200	33.6319	1.4403

Table B2: Values of distance crushed during peak load

Fibre Sequence	Triggering Mechanism	Length of specimen crushed in post-crushing zone (mm)				
		Specimen			Average	Std. Dev
		1	2	3		
GGG	No	0.8757	0.8046	0.2662	0.6488	0.2721
	45 Chamfer	9.1966	10.2029	9.2177	9.5391	0.4695
	Tulip	29.2501	30.2334	26.9501	28.8112	1.3759
GBG	No	2.2623	1.8667	2.1667	2.0986	0.1685
	45 Chamfer	9.9001	10.8166	9.7000	10.1389	0.4861
	Tulip	27.1166	27.6667	27.7501	27.5111	0.2810
BGB	No	4.9000	3.7000	2.7833	3.7945	0.8667
	45 Chamfer	5.1833	5.9833	6.0543	5.7403	0.3949
	Tulip	29.9167	22.3166	20.0333	24.0889	4.2250
BBB	No	4.5834	4.2834	4.2317	4.3661	0.1550
	45 Chamfer	19.5479	19.6216	19.9334	19.7010	0.1671
	Tulip	23.2501	19.8335	9.7834	17.6223	5.7157

Table B3: Mean load values

Fibre Sequence	Triggering Mechanism	Mean Load (kN)				
		Specimen			Average	Std. Dev
		1	2	3		
GGG	No	19.2714	19.7842	19.2106	19.4221	0.25727
	45 Chamfer	19.2203	19.4780	21.5439	20.0807	1.03996
	Tulip	22.6321	22.3869	21.2295	22.0828	0.61166
GBG	No	35.5665	37.4123	35.6587	36.2125	0.84921
	45 Chamfer	37.4934	37.7577	37.6608	37.6373	0.10915
	Tulip	40.2556	41.8074	39.4907	40.5179	0.9638
BGB	No	36.3627	35.4981	30.3870	34.0826	2.63692
	45 Chamfer	38.5184	35.5443	39.5393	37.8674	1.6947
	Tulip	38.7319	41.4968	39.0870	39.7719	1.22826
BBB	No	20.3363	20.6015	20.0656	20.3345	0.21879
	45 Chamfer	21.6997	22.7467	21.9318	22.1261	0.449
	Tulip	31.7872	27.5121	21.3397	26.8797	4.28854

Table B4: Length of specimen crushed in post-crushing zone

Fibre Sequence	Triggering Mechanism	Values of distance crushed during peak load (mm)				
		Specimen			Average	Std. Dev
		1	2	3		
GGG	No	84.1243	84.1954	84.7338	84.3512	0.2721
	45 Chamfer	75.8034	74.7971	75.7823	75.4609	0.4695
	Tulip	55.7499	54.7666	58.0499	56.1888	1.3759
GBG	No	82.7377	83.1333	82.8333	82.9014	0.1685
	45 Chamfer	75.0999	74.1834	75.3000	74.8611	0.4861
	Tulip	57.8834	57.3333	57.2499	57.4889	0.2810
BGB	No	80.1000	81.3000	82.2167	81.2055	0.8667
	45 Chamfer	79.8167	79.0167	78.9457	79.2597	0.3949
	Tulip	55.0833	62.6834	64.9667	60.9111	4.2250
BBB	No	80.4166	80.7166	80.7683	80.6339	0.1550
	45 Chamfer	65.4521	65.3784	65.0666	65.2990	0.1671
	Tulip	61.7499	65.1666	75.2166	67.3777	5.7157

Table B5: Specific Energy Absorption values

Fibre Sequence	Triggering Mechanism	Specific Energy Absorption (kJ/kg)				
		Specimen			Average	Std. Dev
		1	2	3		
GGG	No	18.4227	18.9289	18.71021	18.6873	0.2073
	45 Chamfer	20.2356	18.4417	22.0628	20.2467	1.4783
	Tulip	22.9406	22.2919	22.00659	22.4131	0.3908
GBG	No	24.3198	25.0823	24.41096	24.6043	0.3400
	45 Chamfer	23.2707	22.4079	29.54015	25.0729	3.1784
	Tulip	27.4133	28.1994	26.59808	27.4036	0.6538
BGB	No	25.5496	26.7221	23.34874	25.2068	1.3983
	45 Chamfer	28.4668	27.5352	29.44774	28.4833	0.7809
	Tulip	25.0998	30.9662	30.59467	28.8869	2.6822
BBB	No	13.5155	14.4598	12.09449	13.3566	0.9722
	45 Chamfer	10.5207	11.2663	12.40892	11.3986	0.7765
	Tulip	19.8268	19.0731	15.89208	18.2640	1.7052

Table B6: Crush Force Efficiency values

Fibre Sequence	Triggering Mechanism	Crush Force Efficiency, CFE				
		Specimen			Average	Std. Dev
		1	2	3		
GGG	No	0.4631	0.3703	0.4828	0.4387	0.0490
	45 Chamfer	1.0859	0.9357	0.7234	0.9150	0.1487
	Tulip	1.2463	1.2396	1.1303	1.2054	0.0532
GBG	No	0.5686	0.7500	0.5819	0.6335	0.0826
	45 Chamfer	0.8277	0.8197	0.9402	0.8625	0.0550
	Tulip	0.8925	0.8682	0.8124	0.8577	0.0335
BGB	No	0.5190	0.7134	0.4598	0.5641	0.1083
	45 Chamfer	0.7635	0.6030	0.7402	0.7022	0.0708
	Tulip	0.8329	0.8790	0.9193	0.8771	0.0353
BBB	No	0.4568	0.4614	0.2461	0.3881	0.1004
	45 Chamfer	0.4224	0.3390	0.5196	0.4270	0.0738
	Tulip	0.9480	0.7762	0.6685	0.7976	0.1151